Decadal to multidecadal variability and the climate change background

Article

Published Version

JOURNAL OF GEOPHYSICAL RESEARCH, VOL. 112, D18115, doi:10.1029/2007JD008411, 2007

Decadal to multidecadal variability and the climate change background

David Parker,[1] Chris Folland,[1] Adam Scaife,[1] Jeff Knight,[1] Andrew Colman,[1] Peter Baines,[2,3] and Buwen Dong[4,5]

Received 12 January 2007; revised 22 May 2007; accepted 29 June 2007; published 28 September 2007.

[1] Three prominent quasi-global patterns of variability and change are observed using the Met Office's sea surface temperature (SST) analysis and almost independent night marine air temperature analysis. The first is a global warming signal that is very highly correlated with global mean SST. The second is a decadal to multidecadal fluctuation with some geographical similarity to the El Niño–Southern Oscillation (ENSO). It is associated with the Pacific Decadal Oscillation (PDO), and its Pacific-wide manifestation has been termed the Interdecadal Pacific Oscillation (IPO). We present model investigations of the relationship between the IPO and ENSO. The third mode is an interhemispheric variation on multidecadal timescales which, in view of climate model experiments, is likely to be at least partly due to natural variations in the thermohaline circulation. Observed climatic impacts of this mode also appear in model simulations. Smaller-scale, regional atmospheric phenomena also affect climate on decadal to interdecadal timescales. We concentrate on one such mode, the winter North Atlantic Oscillation (NAO). This shows strong decadal to interdecadal variability and a correspondingly strong influence on surface climate variability which is largely additional to the effects of recent regional anthropogenic climate change. The winter NAO is likely influenced by both SST forcing and stratospheric variability. A full understanding of decadal changes in the NAO and European winter climate may require a detailed representation of the stratosphere that is hitherto missing in the major climate models used to study climate change.

Citation: Parker, D., C. Folland, A. Scaife, J. Knight, A. Colman, P. Baines, and B. Dong (2007), Decadal to multidecadal variability and the climate change background, *J. Geophys. Res.*, *112*, D18115, doi:10.1029/2007JD008411.

1. Introduction

[2] In this paper we first discuss the character of current global warming. We then review the most prominent modes of climate variability seen in the instrumental record and compare these to the background signal of global warming which appears to be almost independent. The first mode is the quasi-global manifestation of the Pacific Decadal Oscillation [*Mantua et al.*, 1997] as described by *Power et al.* [1999] and *Folland et al.* [2002]. The second mode is the quasi-interhemispheric or Atlantic Multidecadal mode which is likely to be partly related to variations in the thermohaline circulation [e.g., *Kerr*, 2000; *Delworth and Mann*, 2000; *Knight et al.*, 2005] and in recent decades also influenced by the changing distribution of anthropogenic aerosols [*Rotstayn and Lohmann*, 2002; *Stott et al.*, 2006]. Both modes were found in temperature data by *Mann and Park* [1994] and in multivariate analyses of oceanic variability by *Mann and Park* [1996], *Folland et al.* [1999] and *Cai and Whetton* [2001]. Such modes of variability must be taken into account when considering climate change on decadal to interdecadal timescales. Regionally many other modes of variability vary on decadal timescales, e.g., the Northern Annular Mode or Arctic Oscillation, the Southern Annular Mode or Antarctic Oscillation, and the Asian and West African monsoons. In this paper we single out the winter North Atlantic Oscillation because of its remarkable multidecadal increase between about 1965 and 1995 which had large effects on regional climate [*Scaife et al.*, 2005, 2007]. We discuss the relationship between these effects, on both mean climate and on extremes, and anthropogenic climate forcing.

[3] Finally we discuss conceptually how the interactions of natural modes of decadal to interdecadal climate variability and anthropogenically induced climate change can cause regional climate surprises. This is exemplified by the possibly anthropogenic recent increase in the NAO [*Shindell et al.*, 1999], resulting in winter NAO warming in northern Europe

[1] Hadley Centre, Met Office, Exeter, UK.
[2] Department of Civil and Environmental Engineering, University of Melbourne, Melbourne, Victoria, Australia.
[3] Also at Quantifying and Understanding the Earth System, Department of Earth Sciences, University of Bristol, Bristol, UK.
[4] Walker Institute for Climate System Research, University of Reading, Reading, UK.
[5] Also at National Centre for Atmospheric Science-Climate, Reading, UK.

over and above the background anthropogenic warming during about 1965–1995. Another example is the likely simultaneous anthropogenic and thermohaline circulation induced warming of the North Atlantic ocean surface and subsurface since 1985, as shown by *Trenberth and Shea*'s [2006] finding of residual warming of the surface of the North Atlantic after removing the (nonlinear) global warming trend. This type of climatic interaction is a little explored topic which lies at the heart of attempts at the decadal forecasting of climate that are just starting.

2. Data and Methods

[4] We use land surface air temperature (LSAT) and sea surface temperature (SST) from the noninterpolated combined land surface air and sea surface temperature data set HadCRUT3 of *Brohan et al.* [2006] who used SST from *Rayner et al.* [2006]. The night marine air temperature data (NMAT) are from the optimally interpolated data set of *Rayner et al.* [2003] which excludes parts of the Southern Ocean; they are used in preference to noninterpolated NMAT data following the recommendations of *Folland et al.* [2003]. All these data are anomalies from the average for the climatological reference period, 1961–1990.

[5] To diagnose the leading geographical patterns of decadal to multidecadal variability at the ocean surface, we calculated covariance empirical orthogonal functions (EOFs) for the period 1891 to 2005. We calculated these EOFs using low-pass-filtered successive seasonal (January to March 1891, April to June 1891 etc.) temperature anomalies, relative to 1961–1990, for almost-equal-area boxes of dimension 10° latitude × 12° longitude at the equator. The use of these large boxes helps to increase the stability of the analysis by increasing the number of time series values relative to the number of boxes. To be included in the analysis, we required that a box have at least 10 contributory monthly 5° × 5° area values in at least 40% of the 3-month seasons. We used a Chebyshev filter with a half-power period of 11 years: this filter has very similar effects to those of the Kalman filter used by *Folland et al.* [1999]. The leading global EOF captures the long-term trends (section 3), leaving the remaining EOFs effectively detrended. We chose the analysis period 1891–2005 to both maximize the ratio of the second to third eigenvalues, preventing the EOFs from being confounded, and to sample a longer period of variability than *Folland et al.* [1999]. Experiments show that the ratio of the eigenvalues of EOF3 to EOF2 should be close to 0.8, or smaller, to prevent confounding of the patterns. *Cai and Whetton*'s [2001] patterns are quite similar to ours, as are those of *Folland et al.* [1999] except that EOFs 2 and 3 are in reverse order. We calculated the principal components of the EOFs for the full period of data, 1850–2006 for LSAT and SST; and 1856–2006 for NMAT. These series, and the global SST and NMAT series plotted with them, were filtered again with the same Chebyshev filter to remove the effects of missing data in the early years without adversely affecting the later parts of the series.

[6] Our remaining plots of geographically averaged temperatures and of Central England temperature [*Parker and Horton*, 2005] use a 21-point binomial filter, which passes decadal and longer-term changes. To create full-length low-pass plots, we use the minimum-slope constraint of *Mann* [2004]; that is, the series are first extended at each end by reflecting the nearest 10 terms about the time boundary of the series.

[7] Assimilations of observed surface wind over the Pacific are taken from the NCEP/NCAR Reanalysis [*Kalnay et al.*, 1996], and observational subsurface Pacific Ocean temperatures are taken from the Simple Ocean Data Assimilation (SODA) of *Carton et al.* [2000]. The North Atlantic Oscillation index is derived from standardized differences of mean sea level pressure between Stykkisholmur (Iceland) and Ponta Delgada (Azores).

[8] For modeling the natural variability of the climate we used HadCM3, a coupled ocean-atmosphere model that does not require adjustment of fluxes at the atmosphere-ocean interface to achieve a stable, realistic climatology [*Gordon et al.*, 2000]. The simulation has constant levels of climate forcing factors such as greenhouse gases, so only contains variability that is internal to the coupled climate system. We also used an enhanced ocean version of HadCM3, HadCEM, which has an oceanic resolution of 1/3° × 1/3°, 40 oceanic levels, and refined treatment of oceanic mixing, diffusion and advection [*Roberts et al.*, 2004]. For studies of the North Atlantic Oscillation we have also used HadGEM1 [*Johns et al.*, 2006, *Ringer et al.*, 2006].

3. Global Warming Background

[9] The best evidence for the magnitude and character of global warming at the Earth's surface is the coincident increase of three almost independent measures of global temperature: land surface air temperature, sea surface temperature and night marine air temperature (Figure 1). Figure 1 is an update of the graph shown by *Folland et al.* [2001b], based on improved data sets. The agreement between SST and NMAT is generally very close, though some NMAT data before 1893 are calibrated against SST data [*Rayner et al.*, 2003]. The greater increase of LSAT in the last 15 years is highly likely to be real. This is shown by a number of studies which found that urbanization has had only a minimal effect on estimates of global-scale land surface air temperature trends [e.g., *Jones et al.*, 1990; *Peterson et al.*, 1999; *Parker*, 2004, 2006]. A small urban warming influence cannot be discounted, but the observed increased warming of the land relative to the oceans is replicated in both transient [*Johns et al.*, 2003] and equilibrium [*Sutton et al.*, 2007] model simulations with increased greenhouse forcing. This, combined with Figure 1, also supports the finding that urban influences on estimated global land surface air temperature trends are at most relatively small (e.g., $\leq$0.1°C [*Jones et al.*, 1990]), though local effects may indeed be much larger. The relatively low land air temperatures around the 1880s and 1890s are a widespread phenomenon in the extratropical Northern Hemisphere [*Parker et al.*, 1994]. Since the oceans account for near 70% of the Earth's surface, SST has the largest role in overall global warming at the surface. SST data over the last decade are increasingly dominated by buoy data in HadSST2; because buoy data are, on average, slightly cooler than ship data [*Reynolds et al.*, 2004; J. Kennedy, personal communication, 2006], global SST trends since about 1990 may have been slightly underestimated. *Brohan*

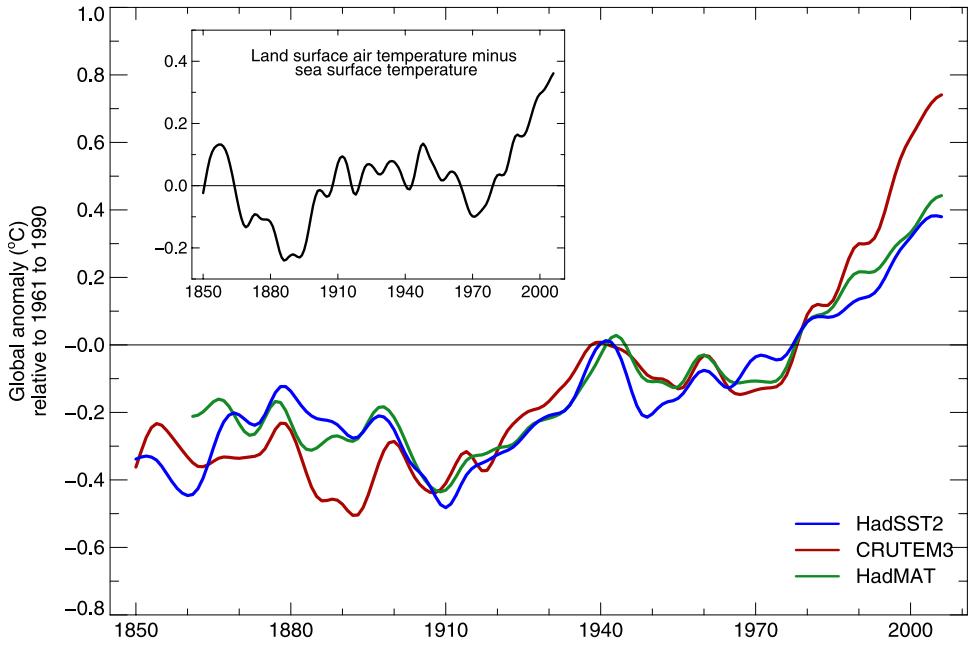

Figure 1. Global land surface air temperature 1850–2006 from CRUTEM3 [*Brohan et al.*, 2006] (red), sea surface temperature 1850–2006 from HadSST2 [*Rayner et al.*, 2006] (blue) and night marine air temperature 1856–2006 from HadMAT [*Rayner et al.*, 2003] (green). The annual data are filtered with a 21 point binomial filter passing variations with a period more than about a decade.

et al. [2006] provide uncertainties in the overall global annual values since 1850 that reflect our current best estimates due to data gaps and data errors. In recent decades, the 5–95% confidence range uncertainties are near ±0.1°C.

[10] We first estimate the overall warming since the beginning of the twentieth century using linear trends as the uncertainties can more readily be estimated. Our uncertainties take account of serial correlation of the annual values, and where available (in our LSAT, SST and blended data and in the *Smith and Reynolds* [2005] data), the uncertainties in the annual values (though not the serial correlation in these uncertainties). To achieve this we use the restricted maximum likelihood linear regression (REML) method [*Diggle et al.*, 1999]. Using this method, we estimate the total warming of LSAT, SST and NMAT for 1901–2006 to be 0.91 ± 0.25°C, 0.71 ± 0.16°C and 0.72 ± 0.14°C respectively where the uncertainties are 5% to 95% confidence intervals. These compare with nonlinear estimates of warming of ∼1.0°C for LSAT and ∼0.75°C for SST and NMAT between 1901–1910 and 1997–2006 using the smooth curves in Figure 1. Combining SST and LSAT, the global mean surface temperature linear trend warming over 1901–2006 [*Brohan et al.*, 2006] is 0.76 ± 0.18°C. Other linear estimates of global surface combined LSAT and SST warming for 1901–2006 using REML are 0.73 ± 0.29°C [*Smith and Reynolds*, 2005] and 0.70 ± 0.13°C [*Hansen et al.*, 2001], though the last value does not include the influence of uncertainties in the annual values as these uncertainties are not available. (Such uncertainties have very little effect on the trend but do modestly widen uncertainties in the trend.) However it is estimated, it is clear that global mean surface warming since the start of the twentieth century has been between 0.7°C and 0.8°C, with 90% confidence range uncertainties that do not exceed 0.2°C. This seems to be a robust result, despite some substantial time-varying data gaps, uncertainties due to time-varying adjustments made in the marine data, residual nonlinearities in the trends, and uncertainties in the land and ocean surface data themselves.

[11] In Figure 2 we illustrate the spatial patterns and temporal behavior associated with global warming at the ocean surface, for comparison with the Pacific and interhemispheric modes shown in sections 4 and 5. The patterns shown in Figure 2 (top) are the leading all seasons covariance EOFs of low-pass-filtered SST and NMAT for 1891–2005 as described in section 2. The projections of these patterns onto the low-pass filtered global SST and NMAT fields for 1850–2006 and 1856–2006 respectively (Figure 2, bottom) are correlated at 0.99 with the seasonal global averages of these fields, confirming that the patterns represent globally coherent warming (or cooling). Our new analysis continues to show changes weakly opposing the global average in the Atlantic near southern Greenland as found by *Folland et al.* [1999], possibly in association with the strengthening of the winter North Atlantic Oscillation between about 1965 and 1995 (section 6).

4. Decadal and Interdecadal Variability in the Pacific

4.1. Interdecadal Pacific Oscillation

[12] The Pacific Ocean has prominent SST variations on timescales ranging from a few years to decades. Recent observational studies have identified decadal-interdecadal climate variability affecting both the tropical and the mid-latitude Pacific Ocean [*Mann and Park*, 1996; *Mantua et*

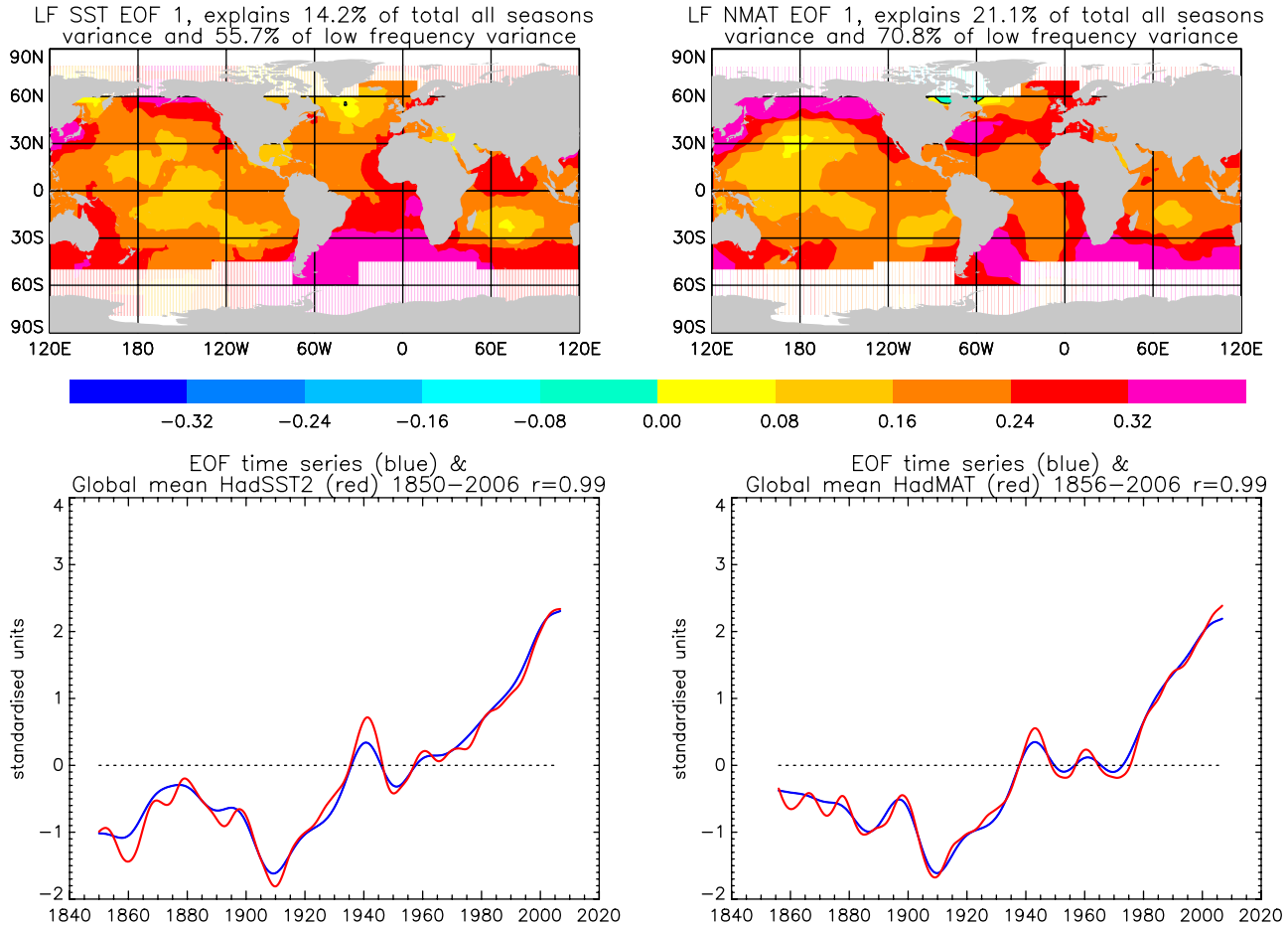

Figure 2. Spatial patterns and temporal behavior associated with global warming at the ocean surface. (top) Leading covariance EOFs of low-pass-filtered (see text) (left) SST and (right) NMAT for 1891–2005 and the variance explained for that period. (bottom) Comparison of the temporal variations of the projections of these patterns onto global fields of low-pass filtered SST for 1850–2006 and NMAT for 1856–2006 (blue) with the global mean anomalies of the low-pass data (red). The horizontal line is the mean of the time series for 1891–2005.

al., 1997; *Zhang et al.*, 1997; *Folland et al.*, 1999; *Power et al.*, 1999; *Mantua and Hare*, 2002; *Allan*, 2006]. In the Pacific Ocean and neighboring regions, patterns of low-frequency fluctuations within the climate and ecological systems have been referred to as the Pacific Decadal Oscillation (PDO) [*Mantua et al.*, 1997; *Mantua and Hare*, 2002], or the Interdecadal Pacific Oscillation (IPO) [*Power et al.*, 1999]. Basically, the PDO has been defined over the North Pacific, while the IPO is seen as wider Pacific basin phenomena, so we use the latter term. The recent work of *Folland et al.* [2002] indicates that the IPO displays signatures at several frequencies [*Mantua and Hare*, 2002] suggestive of a phenomenon ranging across a broad frequency band. *Zhang et al.* [1997] noted that the interdecadal variability in the Pacific SST, from which the interannual component was removed, has a spatial pattern similar to the interannual variability-related pattern except that the meridional scale of tropical anomalies is broader at the decadal timescale.

[13] In Figure 3 we illustrate the spatial patterns and temporal behavior associated with the IPO. Figure 3 (top) shows the second covariance EOFs of low-pass-filtered SST (Figure 3, left) and NMAT (Figure 3, right) for 1891–2005. The two EOFS are quite similar. Figure 3 (bottom) shows the temporal variations of the projections of these patterns onto global SST and NMAT fields for 1850–2006 and 1856–2006 respectively, and imply variability between the ~10-year filter cutoff and ~30 years. In SST, the warmth associated with the warm-equator phase of the IPO extends further west than that associated with El Niño; also IPO has relatively weak variability compared to ENSO in the far eastern tropical Pacific. Furthermore, unlike ENSO, the reversed SST or NMAT anomalies in the midlatitude North Pacific associated with the IPO are as large as those near the equator. In SST, the switch of the IPO from its negative phase to positive phase around 1976 was no larger than the previous, positive to negative, switch in the 1940s; but the 1976 switch was larger than the 1940s switch in NMAT.

[14] The existence of the IPO as a distinct phenomenon has been challenged, e.g., by *Newman et al.* [2003]. They present evidence indicating that the PDO could be a manifestation of the stochastic variability of ENSO pro-

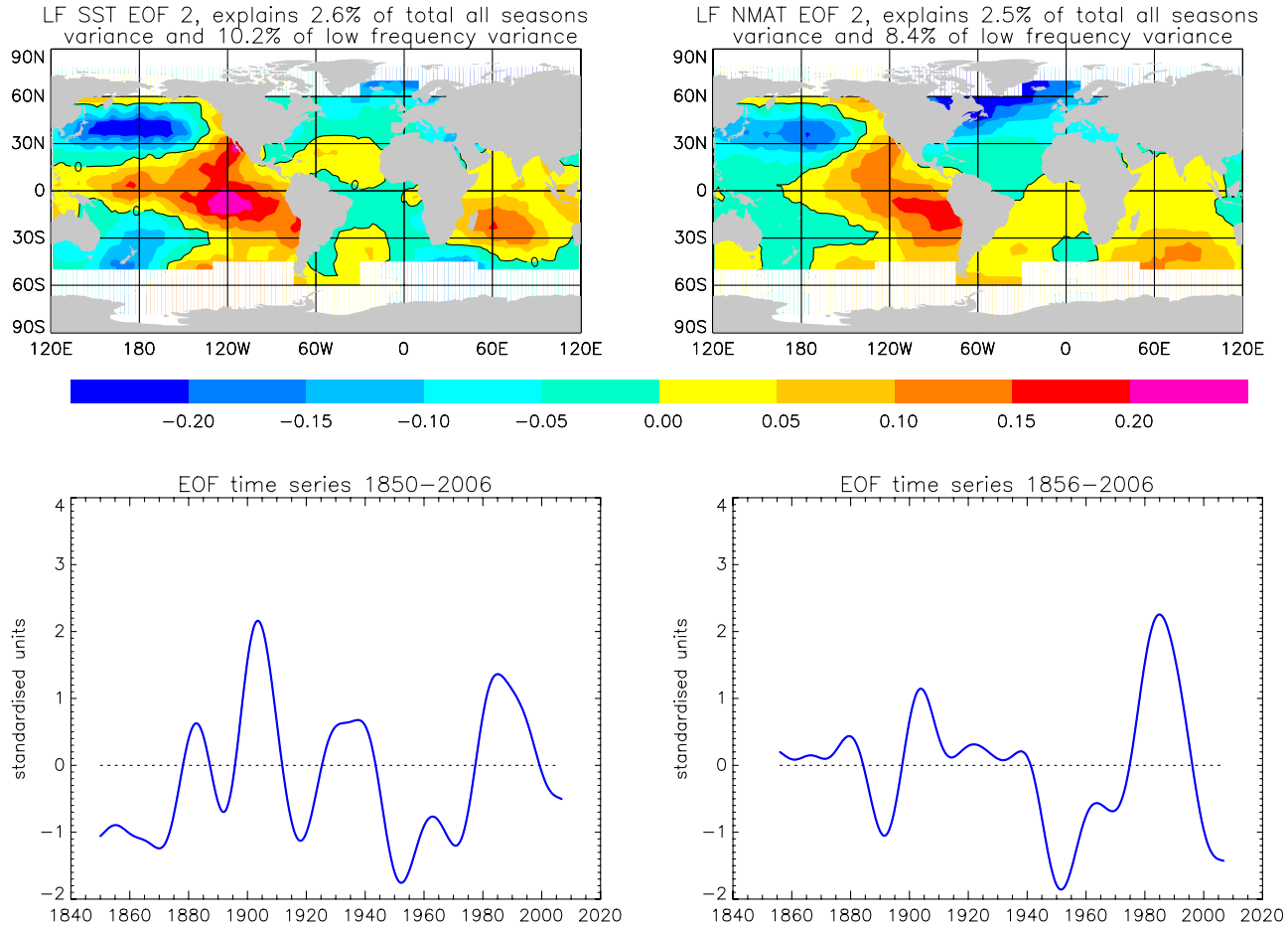

Figure 3. Spatial patterns and temporal behavior of temperature at the ocean surface associated with the Interdecadal Pacific Oscillation. (top) Second covariance EOFs of low-pass-filtered (see text) (left) SST and (right) NMAT for 1891–2005 and the variance explained for that period. (bottom) Temporal variations of the projections of these patterns onto global fields of low-pass-filtered SST for 1850–2006 and NMAT for 1856–2006. The horizontal line is the mean of the time series for 1891–2005.

jected onto decadal to multidecadal timescales. On the other hand, *Folland et al.* [2002], using an analysis of variance technique, showed that the IPO and ENSO had statistically distinguishable effects on the movement of a part of the South Pacific Convergence Zone where there are good data throughout the twentieth century. We explore the nature of the IPO below.

4.2. Modeling the Interdecadal Pacific Oscillation

[15] To understand the IPO, it is necessary to use coupled models. However, we note first that there is quite strong evidence that interannual climatic variability in the tropical Pacific, particularly the El Niño–Southern Oscillation (ENSO) phenomenon, may be modulated on decadal-multidecadal timescales [e.g., *Power et al.*, 1999; *An and Wang*, 2000; *Rodgers et al.*, 2004]. Thus *Meinke et al.* [2005] found considerable evidence of the modulation of worldwide rainfall on the near decadal timescale and some evidence for modulation on multidecadal timescales. Furthermore, various mechanisms have been proposed to explain the origin of decadal-interdecadal variability in the tropical Pacific. These include ocean-atmosphere interactions in the North Pacific [e.g., *Latif and Barnett*, 1996], or the combined extratropical-tropical Pacific [e.g., *Gu and Philander*, 1997; *McPhaden and Zhang*, 2002], and variability within the tropical Pacific domain [e.g., *White et al.*, 2003]. On the other hand, *Power et al.* [2006] have reinterpreted their earlier results in terms of an inherently nonlinear relationship between ENSO and Australian rainfall. They find a much weaker relationship between variations in El Niño strength and Australian rainfall than variations in La Niña strength and Australian rainfall. So they argue that the interpretation by *Power et al.* [1999] of the strongly time varying correlation of ENSO and Australian rainfall as being an influence of a distinct mode of climate variability may not be valid.

[16] Accordingly, in order to understand the nature of the IPO, in particular whether it is independent of ENSO or is merely the stochastic result of interdecadal modulation of ENSO, we have analyzed a 390-year section of the control run of HadCM3 and a 130-year simulation of HadCEM (section 2). The Niño 3 (5°S–5°N, 150–90°W) SST indices based on observations and model simulations are shown in

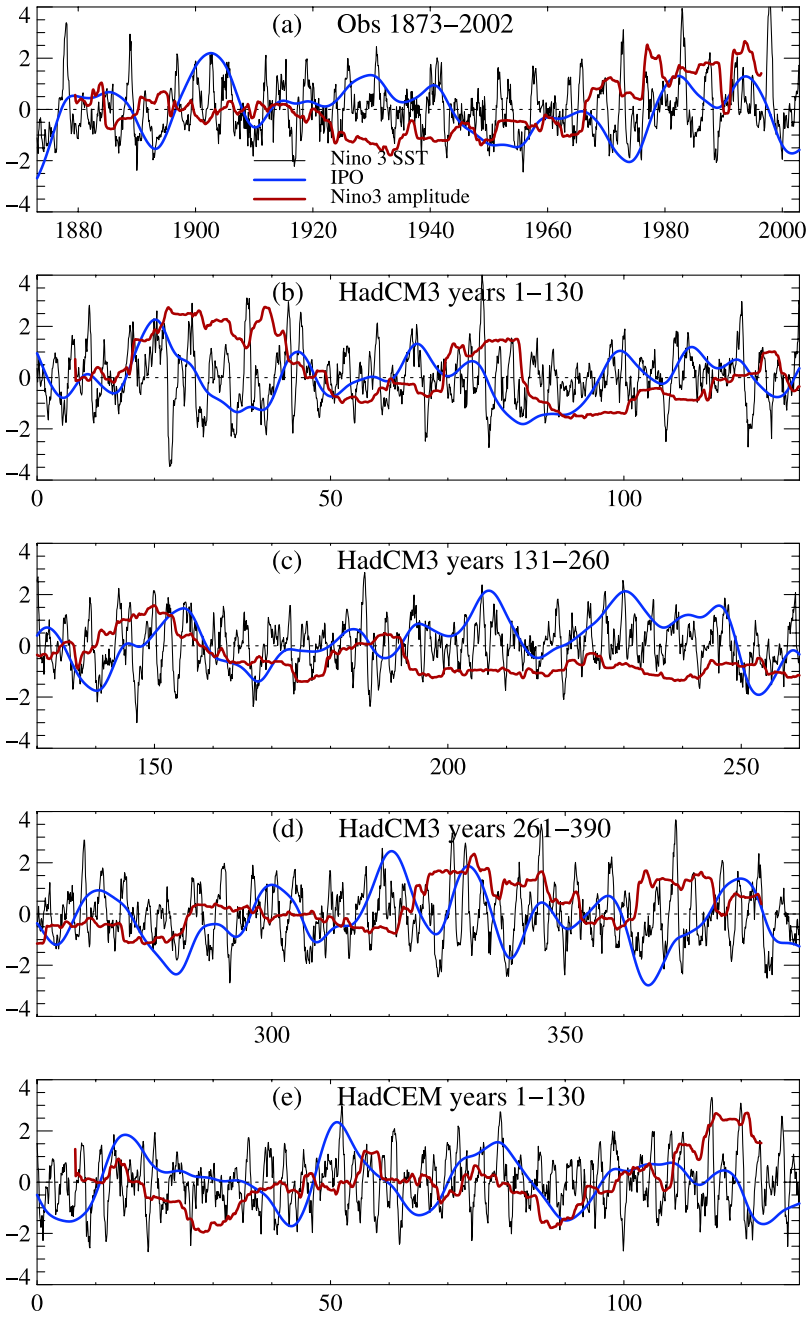

Figure 4. Normalized time series of monthly Niño 3 SST anomalies (thin solid lines), normalized 13-year running variance of Niño 3 SST anomalies (red lines), and the IPO index (blue lines) in (a) observations, (b–d) HadCM3, and (e) HadCEM.

Figure 4. The standard deviations of the monthly mean Niño 3 SST anomalies are 0.88°C and 1.12°C for HadCM3 and HadCEM simulations respectively, compared with an observed value of 0.74°C (1871–2000 [*Rayner et al.*, 2003]). This indicates that HadCM3 simulates eastern Pacific SST fluctuations with realistic magnitude. However, this SST variability may be overestimated by HadCEM by about 25%, though the simulation is too short to assess this well.

[17] Following *Rodgers et al.* [2004], in order to represent low-frequency fluctuations of Niño 3 SST and low-frequency ENSO amplitude modulations, the running 13-year variance of monthly mean Niño 3 SST has been calculated, representing ENSO amplitude modulation (Figure 4). The observational index indicates that the period between 1920 and 1950 was relatively quiescent with respect to ENSO activity, and periods before 1920 and after 1975 were relatively active, e.g., as found by *Kestin et al.* [1998]. An IPO index is also shown in Figure 4. This index is defined from SST data for only the Pacific basin as the Pacific-only IPO SST pattern is similar to the Pacific portion of the global IPO SST pattern in Figure 3, The IPO clearly differs from the low-frequency modulation of ENSO variance. The correla-

tions between the two are 0.22, and −0.03, and 0.37 for observations, HadCM3 and HadCEM, respectively. These weak correlations imply that this measure of the low-frequency modulation of ENSO variability is not directly related to the dominant mode of the low-frequency fluctuation of mean SSTs in the tropical Pacific, especially in the HadCM3 simulation. This fact is supported by analyses based on coral proxy data, which reveal strong decadal/multidecadal variability distinguishable from the decadal/multidecadal modulation of ENSO activity [*Cobb et al.*, 2003].

[18] Nevertheless the two indices may not be completely independent over the last 50 years of observations. The anomalously low SST from 1951 to 1975 is associated with weak interannual SST variability and high SST from 1975 to 2000 is associated with strong interannual SST variability with the two indices being correlated at 0.54. Inspection of HadCM3 results indicates there is no such epoch with high ENSO activity during warm periods and low ENSO activity in cold periods. However, the last 50 years of the HadCEM simulation indicates that high ENSO variability during years 100–130 and low ENSO variability during years 80–100 correspond to warm and cold periods respectively with a correlation coefficient of 0.58 between the low-frequency Niño 3 index and ENSO variance. This may reflect a contribution of SST asymmetry between the El Niño and La Niña phases to the low-frequency SST variability. Nonlinear dynamic heating plays an important role in this asymmetry [*Jin et al.*, 2003], which is captured by HadCEM [*Dong*, 2005], but not by HadCM3 [*Monahan and Dai*, 2004]. During periods of strong ENSO variability, the asymmetry between the El Niño and La Niña is strong (not shown). This leads to a warm residual during the strong ENSO variability period, which in turn may be contributing to low-frequency SST variability.

[19] To illustrate the possible physical processes associated with the IPO, we show in Figure 5 linear regression coefficients relating the IPO index in Figure 4 to surface wind stress and subsurface temperature. Observations indicate anomalous westerlies over the tropics and anomalous cyclonic circulation over the North Pacific when the IPO is positive (Figure 5a), implying weakened easterly trades in the tropical Pacific and a deepened Aleutian low in the North Pacific. The associated subsurface temperature anomalies in the tropical Pacific are characterized by a warmer upper thermocline in the central and eastern tropical Pacific and a colder lower thermocline in the western and central tropical Pacific (Figure 5d). This corresponds to an intensification of the stratification of the equatorial ocean, sharpening the thermocline, and a reduction of its zonal slope. Thus, the IPO mode is reinforced by positive feedbacks in the tropical atmosphere-ocean similar to ENSO feedbacks. Figure 5d also shows changes in near surface temperature on the equator which appear decoupled from the changes in the thermocline in the western and central tropical Pacific. The shallow extent and spatial pattern of the surface positive anomalies suggest that these temperature changes are likely to be a response to reduced evaporation resulting from the weakened easterly trades. The cold temperature anomalies in the western tropical Pacific around the depth of the mean thermocline, associated with a slight shallowing of the thermocline, are likely to be partly a dynamical response to the weakened easterly trade winds in the equatorial tropical Pacific. In addition, the strengthened cyclonic wind stress curl around 15°S enhances the Ekman pumping and raises the thermocline there, leading to cold subsurface temperature anomalies. These cold anomalies could reach the tropics by subduction [*Gu and Philander*, 1997].

[20] These observed characteristics are captured in both HadCM3 and HadCEM model simulations (Figures 5b, 5c, 5e, and 5f). This indicates that model simulated interdecadal variability involves coupled processes similar to ENSO. Figure 5c also indicates that circulation changes in the northern extratropics associated with the IPO are stronger in HadCEM, implying sensitivity to oceanic model resolution. In addition, the anomalous cyclonic wind stress curl around 10°S and 10°N is confined to the western Pacific. As a result, the subsurface cold anomalies are also confined to the western tropical Pacific in HadCEM. Like the observations, HadCM3 shows relatively large atmospheric circulation changes in the Southern Hemisphere (Figure 5b). This may be associated with changes of the South Pacific Convergence Zone (SPCZ) on interdecadal timescales as suggested by *Folland et al.* [2002].

[21] Finally, further insights can be gained from the results of *Arblaster et al.* [2002] who ran the coupled National Center for Atmospheric Research Parallel Climate Model (PCM) for 300 years in control mode, i.e., with fixed greenhouse gases. The atmospheric component of PCM has a horizontal resolution of T42 and 18 levels; the oceanic component has 0.5° latitude resolution at the equator. *Arblaster et al.* [2002] looked for evidence of the IPO mode and the modulation by the IPO of teleconnections to Australian rainfall observed by *Power et al.* [1999]. On timescales exceeding 13 years, the IPO was the first eigenvector of model SST between 60°N and 40°S, with a pattern similar to the IPO mode of *Folland et al.* [1999]. Although modulation was not so great as observed, *Arblaster et al.* [2002] also found that correlations between the model IPO index and modeled Australian rainfall varied in the same way as in the work by *Power et al.* [1999]. These had greater statistical significance because the 300 year simulation was much longer than the 100 years of obser-

Figure 5. (a–c) Regression coefficients of annual mean surface wind stress (surface wind for observations) and (d–f) subsurface ocean temperature in the equatorial Pacific (5°S–5°N) on an index of the Interdecadal Pacific Oscillation. The index is defined using the leading principal component (PC1) of detrended Pacific basin SST filtered to pass variations on longer than decadal timescales. Observations (NCEP [*Kalnay et al.*, 1996] and SODA [*Carton et al.*, 2000]) are shown in Figures 5a and 5d; simulations by HadCM3 are shown in Figures 5b and 5e, and simulations by HadCEM are shown in Figures 5c and 5f. Shading indicates significance at the 5% level. The heavy line in Figures 5d–5f indicates the average depth of the 20°C isotherm in the observations (Figure 5d) and models (Figures 5e and 5f).

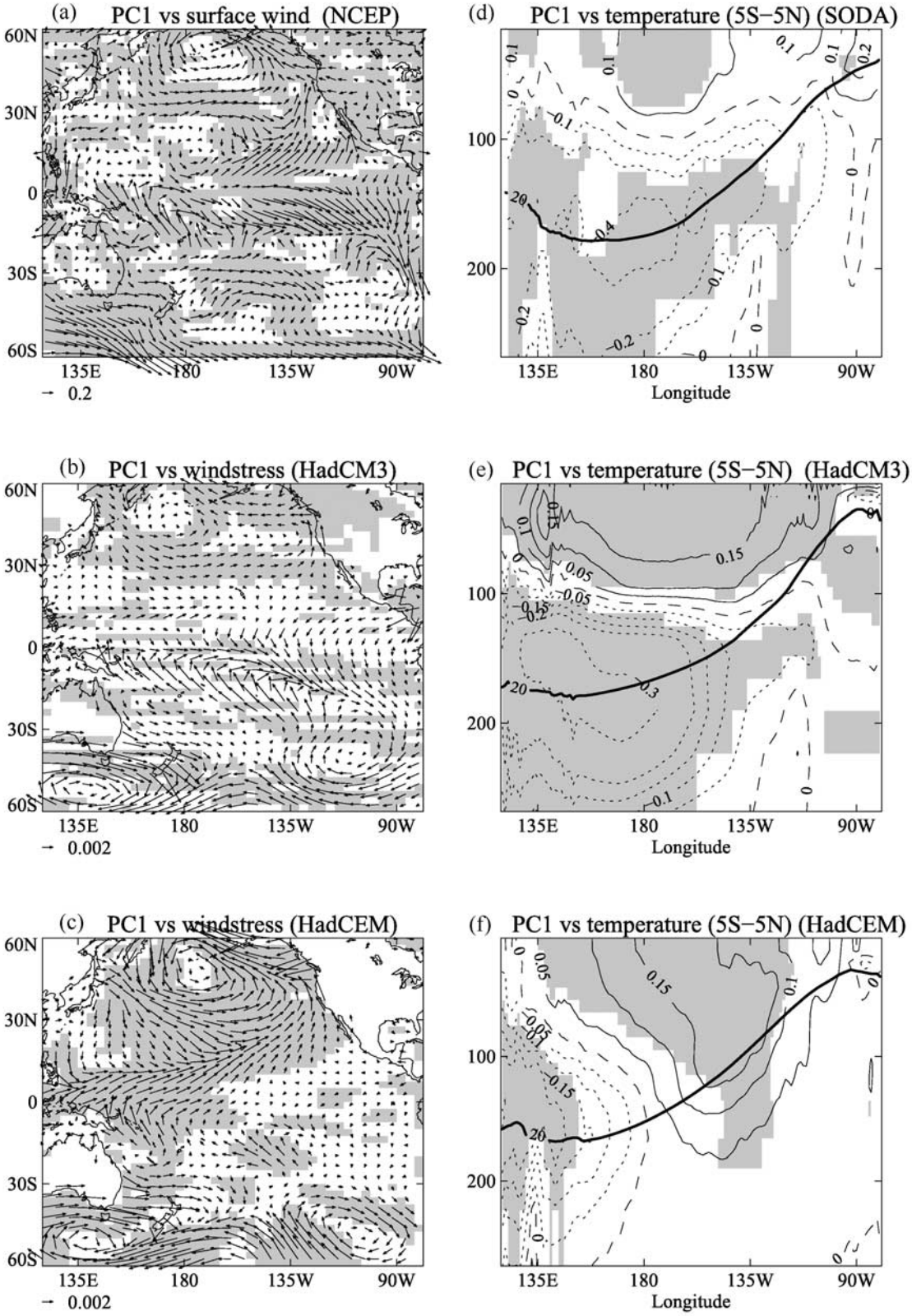
(a) PC1 vs surface wind (NCEP)
60N
30N
0
30S
60S
135E
180
135W
90W
0.2
(b) PC1 vs windstress (HadCM3)
0.002
(c) PC1 vs windstress (HadCEM)
0.002
(d) PC1 vs temperature (5S−5N) (SODA)
100
200
Longitude
(e) PC1 vs temperature (5S−5N) (HadCM3)
Longitude
(f) PC1 vs temperature (5S−5N) (HadCEM)
Longitude

Figure 5

vations. The modulation appeared to be related to the greater El Niño/La Niña variance during negative phases of the IPO in the model related to a shallower model eastern tropical Pacific thermocline. So this is one way such correlations can be modulated. However, our HadCM3/HadCEM results do not fully reflect such a relationship, nor do the observations (Figure 4).

[22] *Arblaster et al.* [2002] also investigated possible physical mechanisms in the model atmosphere for variations in the teleconnections between Australian rainfall and ENSO. They identified one particular possibility, that the IPO modulates these teleconnections through systematic changes in the Walker circulation. In the composite of positive model IPO years, the center of rising motion shifted eastward into the central Pacific and away from Australia. During negative periods, the center of the rising motion shifts west toward Australia, strengthening the relationship between ENSO and Australian precipitation.

[23] In summary, we find that the tropical physical processes involved in the IPO are similar to those driving ENSO. Although ENSO variance is not closely related to the IPO, it is possible that the IPO could simply be a lagged signature of ENSO in the off-equatorial ocean owing, for example, to changes in the frequency of El Niño and La Niña events.

5. Atlantic Multidecadal Oscillation

5.1. Observational and Modeling Background

[24] The idea that climate variability in the North Atlantic sector on decadal and longer timescales could be related to slow changes in the ocean circulation dates back to *Bjerknes* [1964]. Similarly, it had long been speculated that low-frequency sea surface temperature (SST) changes may be responsible for the interdecadal and multidecadal variability of climate in adjacent continental areas. *Folland et al.* [1986] linked the emergence of increased drought in Sahelian Africa to a global pattern of twentieth-century SST fluctuations centered on the Atlantic Ocean. The ability of historical SST data to demonstrate these connections was crucially dependent on the development of new data sets which for the first time used rigorous methods for interpreting the instrumental record [*Folland et al.*, 1984]. Later, *Schlesinger and Ramankutty* [1994] and *Mann and Park* [1994] inferred a 65–70 year period in historical global mean temperature that resulted from the modulation of a similar pattern to that identified by *Folland et al.* [1986]. *Kushnir* [1994] elaborated on the SST pattern, and suggested connections with atmospheric circulation variability, while *Delworth et al.* [1993] showed that a General Circulation Model (GCM) simulation produced 50-year cycles in North Atlantic SST via changes in the Atlantic overturning circulation. The pattern of observed multidecadal SST variations has come to be called the "Atlantic Multidecadal Oscillation" or AMO [*Kerr*, 2000]. Indications that the AMO has been a persistent feature of North Atlantic climate have been provided by paleoclimate data [*Delworth and Mann*, 2000; *Gray et al.*, 2004] which show a signal over about the past 400 years. A range of regional climate variability phenomena beyond Sahel rainfall have subsequently been linked to the AMO, including northeast Brazil rainfall [*Knight et al.*, 2006], North American [*Enfield et al.*, 2001] and European summer climate [*Sutton and Hodson*, 2005; *Pohlmann et al.*, 2006], the Asian summer monsoon [*Goswami et al.*, 2006; *Zhang and Delworth*, 2006; *Lu et al.*, 2006], the austral winter Hadley circulation over the South Atlantic [*Baines and Folland*, 2007], Atlantic hurricane formation [*Goldenberg et al.*, 2001], and ENSO variability [*Dong et al.*, 2006].

[25] The AMO appears in the third covariance EOFs for 1891–2005 of low-pass-filtered SST and NMAT (Figure 6), as part of an interhemispheric dipole. The dipolarity may have arisen in part from the requirement that this EOF must be orthogonal to the first EOF (the secular warming signal in Figure 2), which has the same sign nearly everywhere. However, we note that the simple superposed epoch analysis of *Folland et al.* [1986] also supports a dipolar pattern. The AMO in SST shows alternating warm and cool phases lasting a few decades, particularly 1905–1925 (cool), 1925–1970 (warm) and 1970–2000 (cool), with similar but not identical dates for NMAT. Warm phases are associated with positive temperature anomalies in parts of the North Pacific and in much of North America, Europe, Africa and southern Asia [*Knight et al.*, 2005]. This implies that the AMO is a coherent climate oscillation over much of the Northern Hemisphere. The current state of the AMO, which is just positive compared to the 1891–2005 average, is consistent with the analysis of *Trenberth and Shea* [2006] relative to their base period of 1901–1970. In our analysis, the spatially varying and temporally nonlinear influence of global warming has been removed from the AMO through the isolation of EOF1.

[26] A clear difficulty with assessing whether the AMO is a genuine long-lived climate mode is the shortness of the instrumental record compared to the multidecadal timescales of interest. Palaeoclimate data hint at its existence over the last several centuries [*Delworth and Mann*, 2000; *Gray et al.*, 2004], but these data have considerable uncertainties [*Folland et al.*, 2001b]. *Knight et al.* [2005] provide further insight into the AMO variations shown in Figure 6 by examining a 1400 year control simulation with HadCM3, a coupled ocean-atmosphere model that does not require adjustment of fluxes at the atmosphere-ocean interface to achieve a stable, realistic climatology [*Gordon et al.*, 2000]. The simulation has constant levels of climate forcing factors such as greenhouse gases, so only contains variability that is internal to the coupled climate system. They demonstrate joint variability in the simulated strength of the Atlantic overturning circulation and an AMO-like pattern of surface temperature variability with a near-centennial timescale. The similarities in the pattern, amplitude and timescale of the variability in their model simulation and observations suggests the AMO is a long-lived internal mode of the climate system.

5.2. Modeling the AMO

[27] We show the temperature anomalies associated with the centennial Meridional Overturning Circulation (MOC) mode in HadCM3 using lagged regressions of decadal mean annual surface air temperature with the decadal MOC index (Figure 7). Regressions are calculated for temperature leading and lagging the MOC by up to 5 decades, or half an MOC cycle. The strongest regressions are found when there is no lag between decadal MOC and temperature,

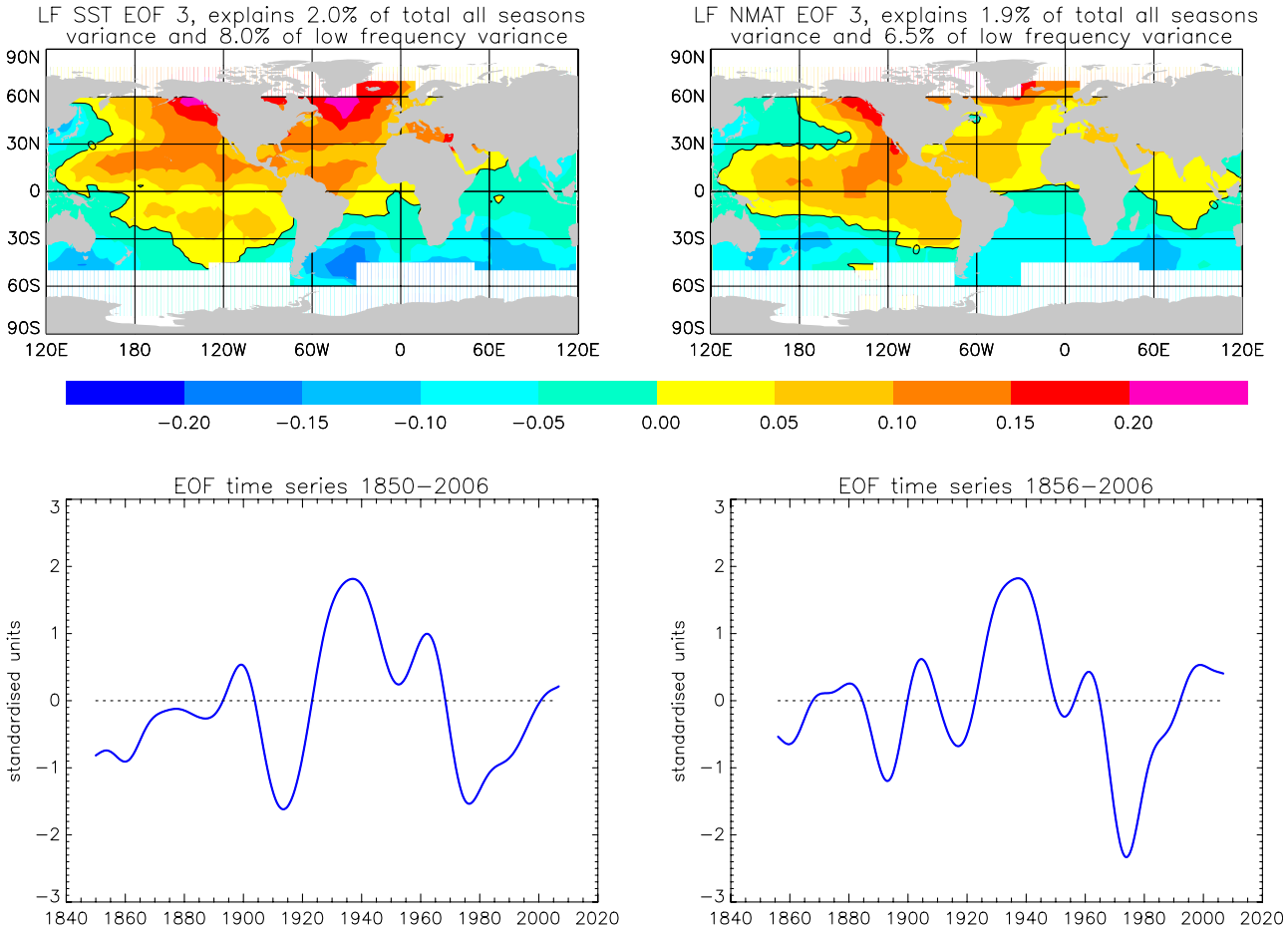

Figure 6. Spatial patterns and temporal behavior of temperature at the ocean surface associated with the Atlantic Multidecadal Oscillation. (top) Third covariance EOFs of low-pass-filtered (see text) (left) SST and (right) NMAT for 1891–2005 and the variance explained for that period. (bottom) Temporal variations of the projections of these patterns onto global fields of low-pass-filtered SST for 1850–2006 and NMAT for 1856–2006. The horizontal line is the mean of the time series for 1891–2005.

implying they vary in phase. The zero-lag pattern shows positive regressions for virtually the entire North Atlantic. This implies that with a weak (strong) MOC, the North Atlantic is cooler (warmer) than average. In addition, the model simulates positive regressions for parts of the North Pacific, western North America, northern South America, Europe, North Africa and much of Asia, suggesting a coherent surface temperature response throughout much of the Northern Hemisphere. Over the oceans, this pattern is very similar to the AMO patterns derived from observed SST and NMAT data in Figure 6. In addition, lagged regression analysis provides a very similar picture to that from the more sophisticated MTM-SVD technique [*Knight et al.*, 2005]. The AMO pattern in HadCM3 diminishes when the MOC leads or lags temperature by a decade, and is essentially not present at leads and lags of 2 decades (Figure 7). On the other hand, when the MOC leads temperature by 4 decades, and to a lesser extent when it lags temperature by 4–5 decades, a pattern of negative regressions is seen that resembles the inverse of the positive pattern seen at zero lag. These are weaker than the zero lag signal, but show that both the AMO and MOC are quasiperiodic, with the potential for some (multi) decadal predictability if initial conditions can be estimated (section 5.4).

5.3. Effects of the AMO on Climate Including the Hadley Circulation

[28] A range of observed regional climate impacts have been linked with the AMO, as described in section 5.1, but the relative shortness of the observational record hampers assessments of the robustness of these links. The demonstration of a realistic AMO signal in the 1400 year model simulation described in section 5.2 permits these observed links to be tested. One such example of regional multidecadal variability is rainfall in northeast Brazil (NEB), where relatively dry (wet) years or decades may be related to a warm (cool) tropical North Atlantic [*Folland et al.*, 2001a] and cool (warm) tropical South Atlantic. Regression of simulated decadal precipitation for the NEB wet season (March–May; MAM) with the MOC index (Figure 8a) shows displacement of precipitation associated with changes in the latitude of the intertropical convergence zone (ICTZ) in response to the AMO/MOC mode. This pattern is consistent with the expected response of the ITCZ to surface

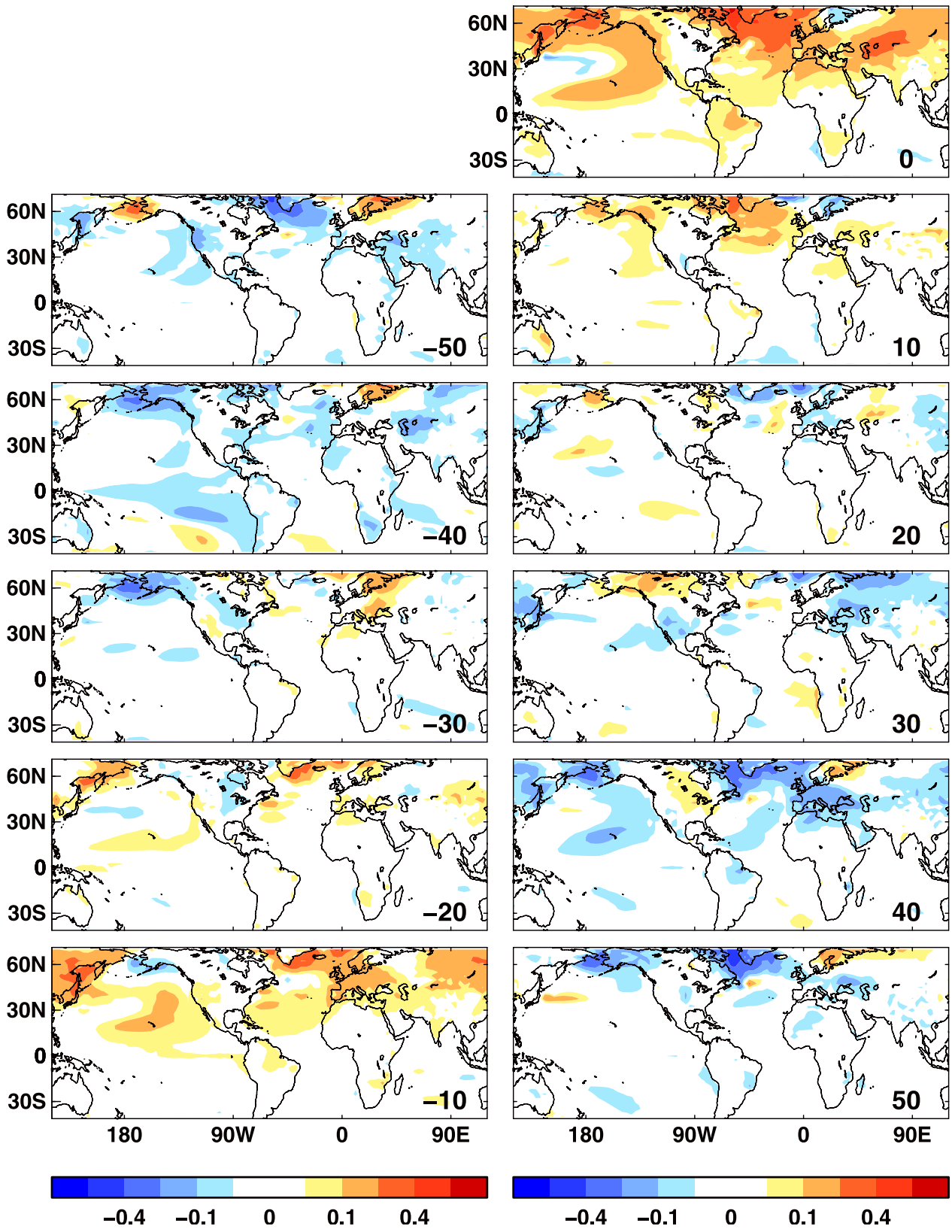

Figure 7. Lagged regression of decadal mean annual surface air temperature with the decadal mean index of the MOC in HadCM3 through a complete centennial cycle. Temperature is shown leading the MOC by 1 to 5 decades in plots marked −10 to −50, in phase with the MOC in the plot marked 0, and lagging the MOC by 1–5 decades in the plots marked 10 to 50. The contour scale is ±0.05, 0.1, 0.2, 0.4, 0.8°C Sv^{-1}. Regressions with magnitude greater that 0.05°C Sv^{-1} are almost entirely significant at the 10% level of a t-test (not shown).

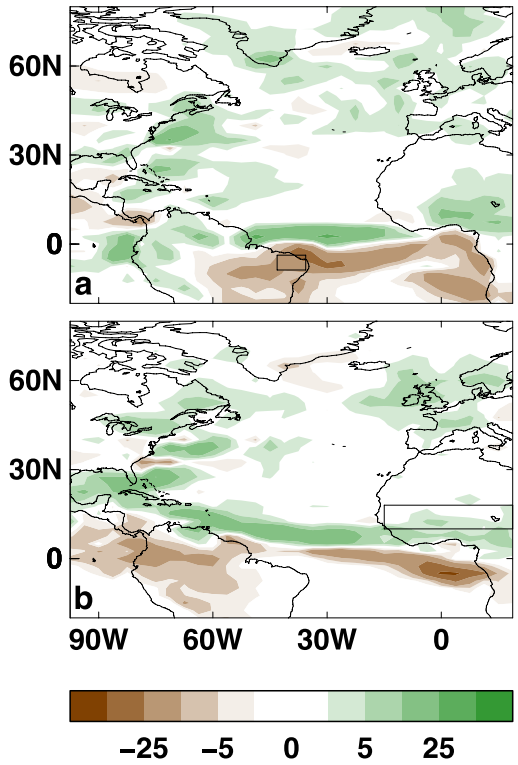

Figure 8. Regression of decadal mean seasonal total precipitation (mm) with decadal mean MOC in HadCM3 for (a) March–May (MAM) and (b) July–September (JAS). The contour scale is ±2, 5, 10, 25, 50 mm Sv^{-1}. In Figure 8a, the northeast Brazil region is outlined, while in Figure 8b, the western Sahel region, including the Soudan (15°W–20°E, 10–18°N) is outlined.

thermal forcing [*Sud et al.*, 2002], and acts to move rainfall away from (toward) NEB in warm (cool) AMO phases. As well as being in the same sense as is observed, the magnitude of the simulated relationship is also consistent with observations [*Knight et al.*, 2006]. A further example of the displacement of the ITCZ in response to the AMO is seen in the model's simulation of precipitation in July–September (JAS) (Figure 8b), which corresponds to the wet season in the African Sahel. The Sahel has experienced large multidecadal rainfall variability, including periods with devastating droughts, which appears to be correlated with the AMO. In the JAS season, the simulated mean ITCZ lies further north than in MAM, near the southern boundary of the Sahel. As such, displacements in the ITCZ can affect Sahel rainfall, with northward (southward) displacements in the warm (cool) AMO phase resulting in wetter (dryer) decades. The simulated amplitude of multidecadal Sahel rainfall variability is less than observed, however, perhaps because of influences from outside the Atlantic [*Lu and Delworth*, 2005], long-term changes in anthropogenic forcings, land surface processes not included in the model, or other model deficiencies. The reduction of Sahel rainfall from a wet 1950s to the dry 1970s and 1980s is nevertheless consistent with the finding of *Baines and Folland* [2007] of a multidecadal weakening of the boreal summer Hadley circulation over the South Atlantic and possibly the North Atlantic during the 1960s. The simulation also provides additional evidence for other observed AMO impacts, such as on European climate and Atlantic hurricane formation [*Knight et al.*, 2006; *Zhang and Delworth*, 2006].

[29] The mechanism of the AMO in HadCM3 has been diagnosed by *Vellinga and Wu* [2004]. An enhanced MOC is associated with greater northward heat transport in the Atlantic and so higher North Atlantic SSTs. This acts to create a northward displacement of the ITCZ which increases freshwater input into the tropical North Atlantic Ocean, creating negative surface salinity anomalies. Over several decades, these anomalies propagate to the northern North Atlantic where they act to suppress oceanic convection and slow the MOC. The next AMO half-cycle then proceeds with the opposite sense of these relationships. Other modeling studies have shown different mechanisms for MOC variability. For example, *Eden and Willebrand* [2001] examine MOC variability in an ocean model driven with historical surface fluxes, finding a lagged response of the MOC to past variations in the North Atlantic Oscillation (NAO). *Delworth and Mann* [2000] also show a connection to the NAO in a coupled framework. In contrast, our coupled simulation does not show an NAO connection at any lead or lag. Persistent interdecadal MOC variability (~25 years timescale) is also apparent in the same HadCM3 simulation [*Dong and Sutton*, 2005], but associated patterns of SST variability are more confined to the northern North Atlantic.

5.4. Prediction of the AMO and Large-Scale Climate

[30] The large scale of the AMO pattern simulated in the model (Figure 7) suggests that the AMO may project onto global and hemispheric mean temperatures. Figure 9 shows the lagged cross correlations of the decadal MOC index with the average decadal mean temperatures for the globe and Northern and Southern Hemispheres. At zero-lag, there

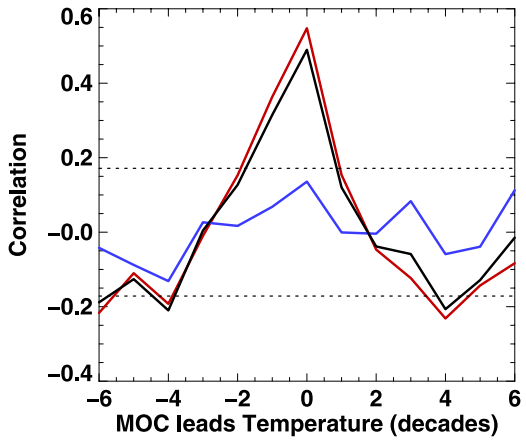

Figure 9. Lagged cross correlations of decadal global (black), Northern Hemisphere (red) and Southern Hemisphere (blue) mean surface temperatures with the MOC index. The 5% confidence limits of correlations statistically significant from zero for the global case are shown as the horizontal dotted lines. The equivalent hemispheric levels are omitted because of similarity with the global case. Negative values on the abscissa indicate temperature leading the MOC.

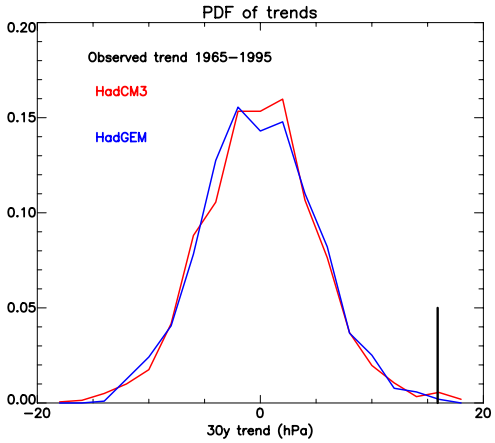

Figure 10. Distribution of modeled 30-year trends in the North Atlantic Oscillation: HadCM3 (red) and HadGEM (blue). The modeled distributions are very similar to each other but have smaller multidecadal trends than the observed NAO trend in 1965–1995 (black).

are significant maximum positive correlations for global (0.49) and Northern Hemisphere (0.55) temperature, in accord with *Zhang et al.* [2007]. The regressions for the globe and Northern Hemisphere are 0.05 ± 0.02°C Sv^{-1} and 0.09 ± 0.02°C Sv^{-1} respectively, implying peak-to-peak variability of 0.1 and 0.2°C. These variations are far from sufficient to explain the observed magnitude of 0.7°C in global warming since 1901 (section 3) and in Northern Hemisphere warming of 0.8°C using the *Brohan et al.* [2006] analysis. However, they are sufficient to contribute to the observed variability in the warming rate, particularly of the Northern Hemisphere. There are no significant correlations with Southern Hemisphere temperature at any lead or lag. As with the overall temperature pattern (Figure 7), there are also significant negative correlations at leads and lags of about 5 decades, or near half an AMO period. This implies that if the temperature anomaly is at a maximum (minimum) in the model, it is statistically likely to be negative (positive) about 50 years later. Hence the existence of the AMO suggests some predictability of large-scale climate and the MOC for several decades into the future. It is possible to make a prediction of the future observed AMO or MOC [*Knight et al.*, 2005], given the recent shift toward a positive AMO phase (Figure 6 and *Trenberth and Shea* [2006]) and allowing for the apparent difference in the periodicity of the AMO in the model and in observations. Such a prediction suggests that the MOC and AMO may peak in the next decade and then decline, resulting in a slowing of the MOC and a temporary cooling influence on the Northern Hemisphere, partly offsetting ongoing warming, particularly in the North Atlantic region and northern Europe, where the MOC-related variability is even larger than for the Northern Hemisphere mean. However, we recognize that our analysis of the AMO in Figure 6 suggests, in agreement with *Trenberth and Shea* [2006], that the most recent values are closer to the zero value than indicated by *Knight et al.* [2005] Therefore the predictions of the future course of the AMO shown by *Knight et al.* [2005] may be more uncertain than they show.

6. Variations in the Winter North Atlantic Oscillation (NAO)

6.1. Winter NAO

[31] The winter NAO [*Hurrell*, 1995] is the single most important pattern of year-to-year variability in atmospheric circulation in the Atlantic sector and its influence extends throughout the Northern Hemisphere via the closely related and highly correlated Arctic Oscillation [*Thompson and Wallace*, 2000]. The NAO appears as a dipolar anomaly in surface pressure with the two centers of action approximately located over Iceland and the Azores. As the NAO increases, there is a northward shift of cyclone tracks, a net decrease in sea level pressure over Iceland and a net increase over the Azores. This pressure difference is often used as a measure of the NAO [*Jones et al.*, 1997] and shows large interannual and interdecadal variability over the last 140 years [*Scaife et al.*, 2005]. Interannual variations of the winter NAO are associated with a "tripole" pattern of North Atlantic SST [*Rodwell and Folland*, 2002]. However, on decadal timescales, *Rodwell et al.* [1999] and *Mehta et al.* [2000] reproduced less than 40% of the trend in the winter NAO between 1965 and 1995 using atmospheric models forced by SST alone. The underestimation of the trend may arise because the observed decadal NAO-SST relationship is representative of the atmosphere forcing the ocean, rather than the ocean forcing the atmosphere [*Bretherton and Battisti*, 2000]. However, we also show in section 6.3 that realistic coupling to the stratosphere is likely to be necessary for simulation of the winter NAO.

6.2. Multidecadal Variability of the Winter NAO in Observations and Models

[32] Minima in the NAO index, such as in the early 1960s, indicate periods of reduced north–south pressure gradient, reduced westerly winds and weaker advection of warm oceanic air onto the cold European landmass. Strongly negative NAO periods like the 1960s also coincide with periods of increased blocking frequency and increased incidence of cold easterlies over Europe [*Shabbar et al.*, 2001].

[33] GCMs reproduce the main features of the pattern and interannual variability of the NAO although there are significant differences between models such as the east-west extent of the NAO [*Osborn*, 2004]. One feature of the observed NAO that is not so well reproduced in models is the multidecadal variability. In particular, the large multidecadal variations in the NAO such as those between the 1960s and 1990s in the observational record have not been reproduced in most models. Neither the internal variability of models [*Osborn*, 2004], nor the inclusion of natural and anthropogenic forcing, appear to be sufficient to easily explain the observations [*Kuzmina et al.*, 2005; *Stenchikov et al.*, 2006]. Figure 10 illustrates this failure to reproduce the magnitude of observed multidecadal variability. The results shown are for very long simulations, with no changes in external forcing, of two different coupled GCMs with completely different dynamical core formulations and numerous differences in physical parameterizations [*Gordon*

et al., 2000; *Johns et al.*, 2006]. These simulations span a combined total of over 4500 years of model simulation but there are only seven 30-year periods (one every 650 years on average and less than 5% of the 30-year periods) when the 30 year trend was as large as the largest 30 year trend seen in the ~150-year observed record. Several of these simulated occurrences also occurred very close together. These results support the studies mentioned above, suggesting that the models and observations may be inconsistent with regard to multidecadal winter NAO variability.

[34] There are various possible reasons for this apparent inconsistency. Model horizontal resolution leading to inaccurate representations of the eddies in the Atlantic storm track is a possibility but the two models in Figure 10 have quite different horizontal resolution and show very similar multidecadal NAO variability, so this is unlikely to be the cause. A second possibility is that SST changes in the tropical Indian and west Pacific oceans have a major influence on the NAO [*Hurrell et al.*, 2004; *Hoerling et al.*, 2004], and that these SST changes, or the consequent changes of atmospheric convection, are not well represented in the models. A third possibility is that the vertical domain of both models is too restricted and that the response of the NAO to stratospheric changes is responsible for the larger observed changes. Following early work by *Boville* [1984] on the response of the troposphere to changes in stratospheric circulation in a GCM, numerous authors have pointed out such a response in observations [e.g., *Kodera and Chiba*, 1995; *Baldwin and Dunkerton*, 2001] and other models [*Norton*, 2003; *Scaife et al.*, 2005]. A similar response has been seen to natural volcanic forcing [*Stenchikov et al.*, 2006] and to anthropogenic greenhouse gas (GHG) forcing [*Shindell et al.*, 1999; *Sigmond et al.*, 2004] although this last aspect is model-dependent [*Gillett et al.*, 2002]. Most current models do not show a consistent or large response of the NAO to changes in GHGs [*Miller et al.*, 2006].

6.3. Effects of the Winter NAO on Surface Mean Climate and on Climate Trends

[35] The winter temperature signal associated with positive NAO is not simply a warming over central and northern Europe: it has a dipolar character with weaker but significant and widespread cooling over the Mediterranean region, over western Asia in these latitudes, and over North Africa. A similar but opposite phased dipole occurs over North America. Over Europe, the temperature changes result partly from the direct effects of a northward shift in storm-track-related cloudiness but mainly from the differences in meridional advection associated with the positive phase of NAO that result in southwesterly (warm) advection in northern European and northeasterly (cold) advection in southern Europe, North Africa and parts of western Asia. Likewise, the precipitation signal with a positive NAO [*Hurrell*, 1995] is an increase over northwestern Europe, especially where southwesterly winds encounter mountains, and a decrease in southern Europe, limiting water resources in Mediterranean regions which rely on winter rainfall.

[36] As models have difficulty in simulating the recent increase in the NAO they also have difficulty in simulating the recent surface climate change around the Atlantic basin. *Scaife et al.* [2005] noted that the area mean temperature trend from an atmospheric model in which all well-known greenhouse gas and natural forcings, including observed SST, were included was still only around 30% of the observed warming over northern Europe between 1965 and 1995. They also noted that the observed polar night jet in the lower stratosphere strengthened significantly over the same period. By relaxing the upper level winds in their model to produce a similar strengthening of the polar night jet, they were able to reproduce a model response in the surface NAO and surface temperature that closely resembled changes seen in the observations. This implies both that the stratosphere is likely to influence the NAO and that the surface climate change over Europe in winter during 1965–1995 is likely to have been dominated by the changes in the NAO. It is therefore important to establish whether the NAO is likely to respond to anthropogenic forcings or whether its variability is likely to be mainly natural in origin. The decrease of the NAO over the last decade to near average levels by 2006 suggests that the increase in the NAO over 1965–1995 was partly natural in origin, but model simulations do also point to an anthropogenic component in the increase [*Shindell et al.*, 1999; *Sigmond et al.*, 2004; *Gillett et al.*, 2005].

[37] Given long records such as the Central England temperature (CET) [*Parker and Horton*, 2005], a statistically significant response to anthropogenic greenhouse gas emissions can be detected on the small spatial scale of CET even in winter [*Karoly and Stott*, 2006]. However, on timescales at least up to 30 years, changes in the NAO appear to be large enough to dominate current estimates of anthropogenic change in winter climate over northern Europe. Climate predictions for Europe in winter therefore need to account for this natural mode of variability if the full range of future regional and seasonal scenarios is to be estimated. The question of whether such multidecadal trends can be simulated realistically with a model with much better stratospheric resolution has yet to be tested.

6.4. Changes in the Winter NAO and Extremes

[38] The incidence of severe wind storms over northwestern Europe is positively correlated with the winter NAO [*Alexander et al.*, 2005] while the frequencies of cold air outbreaks in Europe and western USA are negatively correlated with NAO [*Thompson and Wallace*, 2001]. Heavy precipitation in winter at stations north of 40°N has increased in line with mean precipitation [*Moberg et al.*, 2006], which increases with the winter NAO [*Hurrell*, 2005]. So it is essential when estimating the behavior of extremes, as well as of mean climate, to distinguish the behavior of changes in the winter NAO (whether natural or anthropogenic) from background anthropogenic effects.

[39] An attempt to quantify the effects of the NAO on European climate extremes was made by *Scaife et al.* [2007] using the numerical integrations described in section 6.3 above. These results allowed changes in extremes including changing greenhouse gases but without the NAO perturbation to be compared with those including greenhouse gases and the NAO perturbation. This allowed some assessment of the influence of the observed increase in the NAO on extremes. The results showed that trends in the frequency of both extreme minimum temperature and heavy precipitation events were strongly affected by the changing NAO

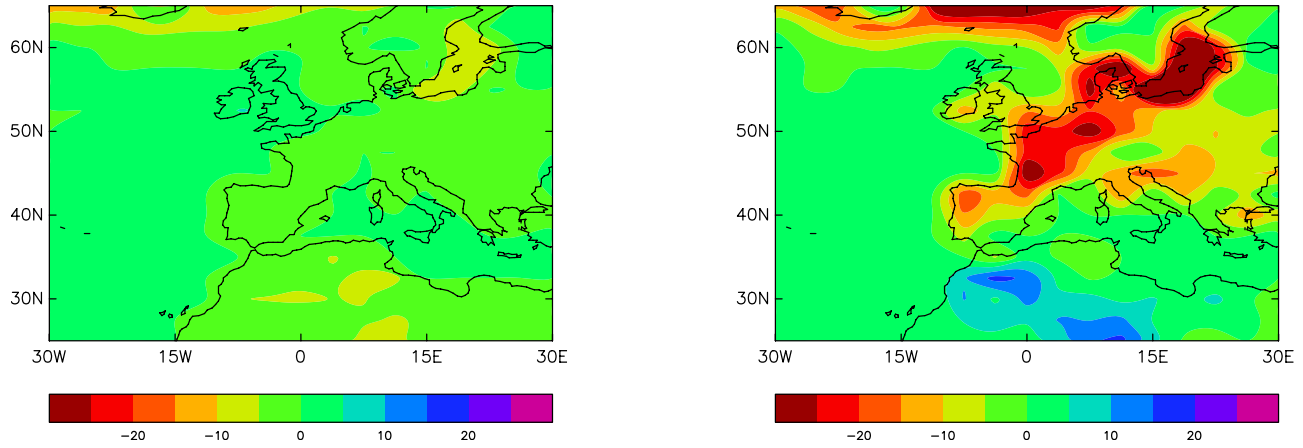

Figure 11. Change in frequency of frosts owing to (left) anthropogenic and natural forcings and (right) anthropogenic and natural forcings plus a 14 hPa change in the NAO. Results are from the 3rd Hadley Centre atmospheric model. From *Scaife et al.* [2007].

between 1965 and 1995. Similarly, Figure 11 shows that the change in the occurrence of frosts (defined as near surface temperature below 0°C on a given day) is also strongly affected by the NAO. There is a much more substantial reduction between 1965 and 1995, as observed, when the NAO change is added. It seems clear from both these results and section 6.3 that a change in the NAO comparable to that observed between the 1960s and 1990s is associated with large changes in many aspects of European climate compared to those of our current best estimates of background anthropogenically forced changes.

7. Conclusions

[40] Our results demonstrate that regional variations in climate result from a range of natural modes of decadal to interdecadal climate variability as well as from anthropogenically induced climate change. We have been quite selective and the complete range is much wider, though all the remaining modes are regional. An important point is that the combination of these influences can cause regional "climate surprises" by enhancing or masking anthropogenic effects. Climate surprises are particularly likely when the two types of influence are in phase. Thus, the strengthening winter NAO between the 1960s and the 1990s, which may itself have been partly anthropogenic, caused substantial winter warming in Europe in addition to the background anthropogenic warming. As a result, apparent winter climate change over northern Europe in particular was very rapid between 1965 and the late 1990s. As another example, the recent strong warming of the surface of the North Atlantic Ocean (Figure 12), by about 0.3°C more than the global

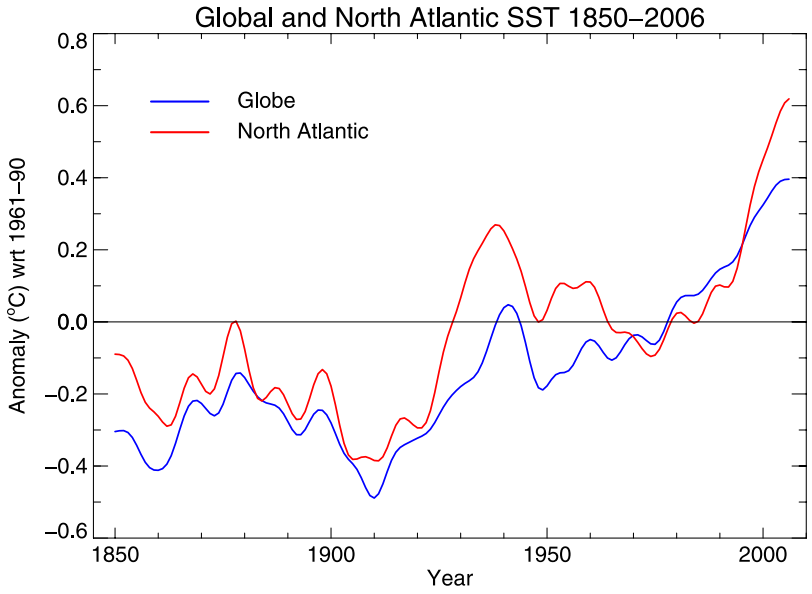

Figure 12. Sea surface temperature anomalies, relative to 1961–1990, since 1850 for the North Atlantic north of the equator (red) and the globe (blue). Annual data from *Rayner et al.* [2006] have been smoothed with a 21-term binomial filter to pass decadal and longer-term variations.

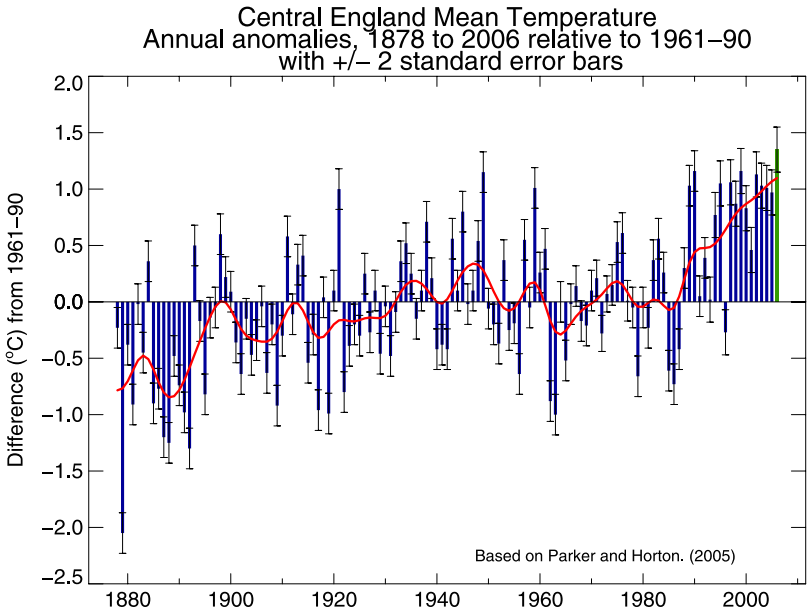

Figure 13. Annual anomalies of Central England temperature, relative to 1961–1990, 1878–2006 (thick bars), with 2σ uncertainty ranges (thin bars), after *Parker and Horton* [2005]. The red curve is the 21 point binomial filtered series. The value for 2006 is shown in green and is the warmest in the record.

average by 2006, is likely to have resulted from a combination of anthropogenic warming and the recovery of the AMO from its negative to a weak positive phase (Figure 6). In turn, variations in the AMO are likely to have influenced the summertime climate over Europe [*Baines and Folland*, 2007]. A particular consequence of in phase AMO and anthropogenic warming over the North Atlantic may have been the exceptional run of recent warm years in the 348-year Central England Temperature record, culminating in a record warm 2006 (Figure 13). CET, being representative of a maritime climate, is likely to be particularly strongly affected by ocean warming, especially warming of the nearby ocean. This nearby warming of SST (not shown) is like that of Figure 12 and even greater recently, and is confirmed by nearby NMAT. *Davies et al.* [1997] demonstrated the strong influence of nearby SST on UK temperatures using a climate model even on the seasonal timescale. The shape of recent CET warming in Figure 13 (a rapid rise from the mid-1980s to about 1995 and a slow rise since then) is likely to have been influenced by rapid warming of the winters to about 1995 due to the NAO changes, and some reversal of that effect since. Successful regional decadal prediction of climate needs to take such interactions into account.

[41] A key element in decadal prediction is to use initial subsurface and surface oceanic conditions to forecast changes in the global distribution of upper and mid-ocean heat content. This requires a multinational commitment to ongoing measurements at and beneath the ocean surface for many decades to come, especially through the Argo Project (http://www.argo.net/) for subsurface ocean floats and through the Voluntary Observing Fleet, as specified in the Implementation Plan for the Global Climate Observing System [*Global Climate Observing System*, 2004]. Development of our understanding of decadal and longer-scale oceanic processes, and of prediction and validation techniques, also requires the digitization of large amounts of manuscript marine surface climate data of many kinds from SST to humidity. A particular problem is the homogenization and reanalysis of historical subsurface ocean temperature data over the last 50 years. Thus suspected quite large time varying biases have yet to be removed or proven to be small. In the meantime, these might significantly affect currently assessed variations in oceanic heat content (M. Palmer, personal communication, 2007). Finally, an integrated observational and modeling approach, as in the review of *Latif et al.* [2006], is essential for diagnosing and predicting regional climate phenomena so that society can adapt to the combined effects of climatic variability and anthropogenic climatic change.

[42] **Acknowledgments.** This work was supported by the CLIVAR Climate of the 20th Century project, the UK Joint Defra and MoD Integrated Climate Programme–GA01101, CBC/2B/0417_Annex C5, and the DYNAMITE project (EU contract 003903-GOCE). This work was carried out under the auspices of the UK government.

References

Alexander, L. V., S. F. B. Tett, and T. Jonsson (2005), Recent observed changes in severe storms over the United Kingdom and Iceland, *Geophys. Res. Lett.*, *32*, L13704, doi:10.1029/2005GL022371.

Allan, R. J. (2006), ENSO and related teleconnections, in *The Global Climate System: Patterns, Processes and Teleconnections*, edited by J. E. Oliver and H. Bridgman, pp. 38–58, Cambridge Univ. Press, New York.

An, S.-I., and B. Wang (2000), Interdecadal change of the structure of the ENSO mode and its impact on ENSO frequency, *J. Clim.*, *13*, 2044–2055.

Arblaster, J. A., G. A. Meehl, and A. M. Moore (2002), Interdecadal modulation of Australian rainfall, *Clim. Dyn.*, *18*, 519–531.

Baines, P. G., and C. K. Folland (2007), Evidence for a rapid global climate shift across the late 1960s, *J. Clim.*, *12*, 2721–2744.

Baldwin, M. P., and T. J. Dunkerton (2001), Stratospheric harbingers of anomalous weather regimes, *Science*, *294*, 581–584.

Bjerknes, J. (1964), Atlantic air-sea interaction, *Adv. Geophys.*, *10*, 1–82.

Boville, B. A. (1984), The influence of the polar night jet on the tropospheric circulation in a GCM, *J. Atmos. Sci.*, *41*, 1132–1142.

Bretherton, C. S., and D. S. Battisti (2000), An interpretation of the results from atmospheric general circulation models forced by the time history of the observed sea surface temperature distribution, *Geophys. Res. Lett.*, *27*, 767–770.

Brohan, P., J. J. Kennedy, I. Harris, S. F. B. Tett, and P. D. Jones (2006), Uncertainty estimates in regional and global observed temperature changes: A new data set from 1850, *J. Geophys. Res.*, *111*, D12106, doi:10.1029/2005JD006548.

Cai, W., and P. H. Whetton (2001), Modes of SST variability and the fluctuation of global mean temperature, *Clim. Dyn.*, *17*, 889–901.

Carton, J. A., G. Chepurin, X. Cao, and B. Giese (2000), A simple ocean data assimilation analysis of the global upper ocean 1950–95. part I: Methodology, *J. Phys. Oceanogr.*, *30*, 294–309.

Cobb, K. M., C. D. Charles, H. Cheng, and R. L. Edwards (2003), El Niño/Southern Oscillation and tropical Pacific climate during the last millennium, *Nature*, *424*, 271–276.

Davies, J. R., D. P. Rowell, and C. K. Folland (1997), North Atlantic and European seasonal predictability using an ensemble of multidecadal atmospheric GCM simulations, *Int. J. Climatol.*, *17*, 1263–1284.

Delworth, T. L., and M. E. Mann (2000), Observed and simulated multidecadal variability in the Northern Hemisphere, *Clim. Dyn.*, *16*, 661–676.

Delworth, T. L., S. Manabe, and R. J. Stouffer (1993), Interdecadal variations of the thermohaline circulation in a coupled ocean-atmosphere model, *J. Clim.*, *6*, 1993–2011.

Diggle, P. J., K. Y. Liang, and S. L. Zeger (1999), *Analysis of Longitudinal Data*, 253 pp., Clarendon, Oxford, U. K.

Dong, B.-W. (2005), Asymmetry between El Niño and La Niña in a global coupled GCM with an eddy-permitting ocean resolution, *J. Clim.*, *18*, 3373–3387.

Dong, B.-W., and R. T. Sutton (2005), Mechanism of interdecadal thermohaline circulation variability in a coupled ocean-atmosphere GCM, *J. Clim.*, *18*, 1117–1135.

Dong, B., R. T. Sutton, and A. A. Scaife (2006), Multidecadal modulation of El Niño–Southern Oscillation (ENSO) variance by Atlantic Ocean sea surface temperatures, *Geophys. Res. Lett.*, *33*, L08705, doi:10.1029/2006GL025766.

Eden, C., and J. Willebrand (2001), Mechanism of interannual to decadal variability of the North Atlantic circulation, *J. Clim.*, *14*, 2266–2280.

Enfield, D. B., A. M. Mestas-Nuñez, and P. J. Trimble (2001), The Atlantic multidecadal oscillation and its relation to rainfall and river flows in the continental US, *Geophys. Res. Lett.*, *28*, 2077–2080.

Folland, C. K., D. E. Parker, and F. E. Kates (1984), Worldwide marine temperature fluctuations 1856–1981, *Nature*, *310*, 670–673.

Folland, C. K., T. N. Palmer, and D. E. Parker (1986), Sahel rainfall and worldwide sea temperatures 1901–85, *Nature*, *320*, 602–607.

Folland, C. K., D. E. Parker, A. W. Colman, and R. Washington (1999), Large scale modes of ocean surface temperature since the late nineteenth century, in *Beyond El Niño: Decadal and Interdecadal Climate Variability*, edited by A. Navarra, pp. 73–102, Springer, New York.

Folland, C. K., A. W. Colman, D. P. Rowell, and M. K. Davey (2001a), Predictability of northeast Brazil rainfall and real-time forecast skill, 1987–98, *J. Clim.*, *14*, 1937–1958.

Folland, C. K., T. R. Karl, J. R. Christy, R. A. Clarke, G. V. Gruza, J. Jouzel, M. E. Mann, J. Oerlemans, M. J. Salinger, and S. W. Wang (2001b), Observed climate variability and change, in *Climate Change 2001: The Scientific Basis—Contribution of Working Group I to the Third Assessment Report of the Intergovernmental Panel on Climate Change*, edited by J. T. Houghton et al., pp. 99–181, Cambridge Univ. Press, New York.

Folland, C. K., J. A. Renwick, M. J. Salinger, and A. B. Mullan (2002), Relative influences of the Interdecadal Pacific Oscillation and ENSO on the South Pacific Convergence Zone, *Geophys. Res. Lett.*, *29*(13), 1643, doi:10.1029/2001GL014201.

Folland, C. K., M. J. Salinger, N. Jiang, and N. A. Rayner (2003), Trends and variations in South Pacific island and ocean surface temperatures, *J. Clim.*, *16*, 2859–2874.

Gillett, N. P., M. R. Allen, and K. D. Williams (2002), The role of stratospheric resolution in simulating the Arctic Oscillation response to greenhouse gases, *Geophys. Res. Lett.*, *29*(10), 1500, doi:10.1029/2001GL014444.

Gillett, N. P., R. J. Allan, and T. J. Ansell (2005), Detection of external influence on sea level pressure with a multi-model ensemble, *Geophys. Res. Lett.*, *32*, L19714, doi:10.1029/2005GL023640.

Global Climate Observing System (2004), GCOS implementation plan for the Global Observing System for Climate in support of the UNFCCC, *Rep. GCOS-92, WMO/TD 1219*, 136 pp., Geneva, Switzerland.

Goldenberg, S. B., C. W. Landsea, A. M. Mestas-Nuñez, and W. M. Gray (2001), The recent increase in Atlantic hurricane activity: Causes and implications, *Science*, *293*, 474–479.

Gordon, C., C. Cooper, C. A. Senior, H. Banks, J. M. Gregory, T. C. Johns, J. F. B. Mitchell, and R. A. Wood (2000), The simulation of SST, sea ice extents and ocean heat transports in a version of the Hadley Centre coupled model without flux adjustments, *Clim. Dyn.*, *16*, 147–168.

Goswami, B. N., M. S. Madhusoodanan, C. P. Neema, and D. Sengupta (2006), A physical mechanism for North Atlantic SST influence on the Indian summer monsoon, *Geophys. Res. Lett.*, *33*, L02706, doi:10.1029/2005GL024803.

Gray, S. T., L. J. Graumlich, J. L. Betancourt, and G. T. Pederson (2004), A tree-ring based reconstruction of the Atlantic Multidecadal Oscillation since 1567 A.D., *Geophys. Res. Lett.*, *31*, L12205, doi:10.1029/2004GL019932.

Gu, D., and S. G. H. Philander (1997), Interdecadal climate fluctuations that depend on exchanges between the tropics and extratropics, *Science*, *275*, 805–807.

Hansen, J., R. Ruedy, M. Sato, M. Imhoff, W. Lawrence, D. Easterling, T. Peterson, and T. Karl (2001), A closer look at United States and global surface temperature change, *J. Geophys. Res.*, *106*, 23,947–23,964.

Hoerling, M. P., J. W. Hurrell, T. Xu, G. T. Bates, and A. S. Phillips (2004), Twentieth century North Atlantic climate change. part II: Understanding the effect of Indian Ocean warming, *Clim. Dyn.*, *23*, 391–405.

Hurrell, J. W. (1995), Decadal trends in the North Atlantic Oscillation: Regional temperatures and precipitation, *Science*, *269*, 676–679.

Hurrell, J. W., M. P. Hoerling, A. S. Phillips, and T. Xu (2004), Twentieth century North Atlantic climate change. part I: Assessing determinism, *Clim. Dyn.*, *23*, 371–389.

Jin, F.-F., S.-I. An, A. Timmermann, and J. Zhao (2003), Strong El Niño events and nonlinear dynamical heating, *Geophys. Res. Lett.*, *30*(3), 1120, doi:10.1029/2002GL016356.

Johns, T. C., et al. (2003), Anthropogenic climate change for 1860 to 2100 simulated with the HadCM3 model under updated emissions scenarios, *Clim. Dyn.*, *20*, 583–612.

Johns, T. C., et al. (2006), The new Hadley Centre climate model (HadGEM1): Evaluation of coupled simulations, *J. Clim.*, *19*, 1327–1353.

Jones, P. D., P. Y. Groisman, M. Coughlan, N. Plummer, W.-C. Wang, and T. R. Karl (1990), Assessment of urbanization effects in time series of surface air temperature over land, *Nature*, *347*, 169–172.

Jones, P. D., T. Jonsson, and D. Wheeler (1997), Extension to the North Atlantic Oscillation using early instrumental pressure observations from Gibraltar and South-West Iceland, *Int. J. Climatol.*, *17*, 1433–1450.

Kalnay, E., et al. (1996), The NCEP/NCAR 40-year reanalysis project, *Bull. Am. Meteorol. Soc.*, *77*, 437–471.

Karoly, D. J., and P. A. Stott (2006), Anthropogenic warming of central England temperature, *Atmos. Sci. Lett.*, *7*, 81–85.

Kerr, R. A. (2000), A North Atlantic climate pacemaker for the centuries, *Science*, *288*, 1984–1985.

Kestin, T. S., D. J. Karoly, J.-I. Yano, and N. A. Rayner (1998), Time-frequency variability of ENSO and stochastic simulations, *J. Clim.*, *11*, 2258–2272.

Knight, J., R. J. Allan, C. K. Folland, M. Vellinga, and M. E. Mann (2005), A signature of persistent natural thermohaline circulation cycles in observed climate, *Geophys. Res. Lett.*, *32*, L20708, doi:10.1029/2005GL024233.

Knight, J. R., C. K. Folland, and A. A. Scaife (2006), Climate impacts of the Atlantic Multidecadal Oscillation, *Geophys. Res. Lett.*, *33*, L17706, doi:10.1029/2006GL026242.

Kodera, K., and M. Chiba (1995), Tropospheric circulation changes associated with stratospheric sudden warmings: A case study, *J. Geophys. Res.*, *100*, 11,055–11,068.

Kushnir, Y. (1994), Interdecadal variations in North Atlantic sea surface temperature and associated atmospheric conditions, *J. Clim.*, *7*, 141–157.

Kuzmina, S. I., L. Bengtsson, O. M. Johannessen, H. Drange, L. P. Bobylev, and M. W. Miles (2005), The North Atlantic Oscillation and greenhouse-gas forcing, *Geophys. Res. Lett.*, *32*, L04703, doi:10.1029/2004GL021064.

Latif, M., and T. P. Barnett (1996), Decadal climate variability over the North Pacific and North America: Dynamics and predictability, *J. Clim.*, *9*, 2407–2423.

Latif, M., M. Collins, H. Pohlmann, and N. Keenlyside (2006), A review of predictability studies of Atlantic sector climate on decadal time scales, *J. Clim.*, *19*, 5971–5987.

Lu, J., and T. L. Delworth (2005), Oceanic forcing of the late 20th century Sahel drought, *Geophys. Res. Lett.*, *32*, L22706, doi:10.1029/2005GL023316.

Lu, R., B. Dong, and H. Ding (2006), Impact of the Atlantic Multidecadal Oscillation on the Asian summer monsoon, *Geophys. Res. Lett.*, *33*, L24701, doi:10.1029/2006GL027655.

Mann, M. E. (2004), On smoothing potentially non-stationary climate time series, *Geophys. Res. Lett.*, *31*, L07214, doi:10.1029/2004GL019569.

Mann, M. E., and J. Park (1994), Global-scale modes of surface temperature variability on interannual to century time scales, *J. Geophys. Res.*, *99*, 25,819–25,833.

Mann, M. E., and J. Park (1996), Joint spatio-temporal modes of surface temperature and sea level pressure variability in the Northern Hemisphere during the last century, *J. Clim.*, *9*, 2137–2162.

Mantua, N. J., and S. R. Hare (2002), The Pacific Decadal Oscillation, *J. Oceanogr.*, *58*, 35–44.

Mantua, N. J., S. R. Hare, Y. Zhang, J. M. Wallace, and R. C. Francis (1997), A Pacific interdecadal climate oscillation with impacts on salmon production, *Bull. Am. Meteorol. Soc.*, *78*, 1069–1079.

McPhaden, M. J., and D. Zhang (2002), Slowdown of the meridional overturning circulation in the upper Pacific Ocean, *Nature*, *41*, 603–608.

Mehta, V. M., M. J. Suarez, J. V. Manganello, and T. L. Delworth (2000), Oceanic influence on the North Atlantic oscillation and associated Northern Hemisphere climate variations: 1959–1993, *Geophys. Res. Lett.*, *27*, 121–124.

Meinke, H., P. de Voil, G. L. Hammer, S. Power, R. Allan, R. C. Stone, C. Folland, and A. Potgieter (2005), Rainfall variability at decadal and longer time scales: Signal or noise?, *J. Clim.*, *18*, 89–96.

Miller, R. L., G. A. Schmidt, and D. T. Shindell (2006), Forced annular variations in the 20th century Intergovernmental Panel on Climate Change Fourth Assessment Report models, *J. Geophys. Res.*, *111*, D18101, doi:10.1029/2005JD006323.

Moberg, A., et al. (2006), Indices for daily temperature and precipitation extremes in Europe analyzed for the period 1901–2000, *J. Geophys. Res.*, *111*, D22106, doi:10.1029/2006JD007103.

Monahan, A. H., and A. Dai (2004), The spatial and temporal structure of ENSO nonlinearity, *J. Clim.*, *17*, 3026–3036.

Newman, M., G. P. Compo, and M. A. Alexander (2003), ENSO-forced variability of the Pacific Decadal Oscillation, *J. Clim.*, *16*, 3853–3857.

Norton, W. A. (2003), Sensitivity of Northern Hemisphere surface climate to simulation of the stratospheric polar vortex, *Geophys. Res. Lett.*, *30*(12), 1627, doi:10.1029/2003GL016958.

Osborn, T. J. (2004), Simulating the winter North Atlantic Oscillation: The roles of internal variability and greenhouse gas forcing, *Clim. Dyn.*, *22*, 605–623.

Parker, D. E. (2004), Large-scale warming is not urban, *Nature*, *432*, 290.

Parker, D. E. (2006), A demonstration that large-scale warming is not urban, *J. Clim.*, *19*, 2882–2895.

Parker, D. E., and E. B. Horton (2005), Uncertainties in central England temperature 1878–2003 and some improvements to the maximum and minimum series, *Int. J. Climatol.*, *25*, 1173–1188.

Parker, D. E., P. D. Jones, C. K. Folland, and A. Bevan (1994), Interdecadal changes of surface temperature since the late nineteenth century, *J. Geophys. Res.*, *99*, 14,373–14,399.

Peterson, T. C., K. P. Gallo, J. Lawrimore, A. Huang, and D. A. McKittrick (1999), Global rural temperature trends, *Geophys. Res. Lett.*, *26*, 329–332.

Pohlmann, H., F. Sienz, and M. Latif (2006), Influence of the multidecadal Atlantic meridional overturning circulation variability on European climate, *J. Clim.*, *19*, 6062–6067.

Power, S., T. Casey, C. Folland, A. Colman, and V. Mehta (1999), Inter-decadal modulation of the impact of ENSO on Australia, *Clim. Dyn.*, *15*, 319–324.

Power, S., M. Haylock, R. Colman, and X. Wang (2006), The predictability of interdecadal changes in ENSO activity and ENSO teleconnections, *J. Clim.*, *19*, 4755–4771.

Rayner, N. A., D. E. Parker, E. B. Horton, C. K. Folland, L. V. Alexander, D. P. Rowell, E. C. Kent, and A. Kaplan (2003), Global analyses of sea surface temperature, sea ice, and night marine air temperature since the late nineteenth century, *J. Geophys. Res.*, *108*(D14), 4407, doi:10.1029/2002JD002670.

Rayner, N. A., P. Brohan, D. E. Parker, C. K. Folland, J. J. Kennedy, M. Vanicek, T. Ansell, and S. F. B. Tett (2006), Improved analyses of changes and uncertainties in sea surface temperature measured in situ since the mid-nineteenth century: The HadSST2 dataset, *J. Clim.*, *19*, 446–469.

Reynolds, R. W., C. L. Gentemann, and F. Wentz (2004), Impact of TRMM SSTs on a climate-scale SST analysis, *J. Clim.*, *17*, 2938–2952.

Ringer, M. A., et al. (2006), The physical properties of the atmosphere in the new Hadley Centre Global Environmental Model (HadGEM1). Part II: Aspects of variability and regional climate, *J. Clim.*, *19*, 1302–1326.

Roberts, M. J., H. Banks, N. Gedney, J. Gregory, R. Hill, S. Mullerworth, A. Pardaens, G. Rickard, R. Thorpe, and R. Wood (2004), Impact of an eddy-permitting ocean resolution on control and climate change simulations with a global coupled GCM, *J. Clim.*, *17*, 3–20.

Rodgers, K. B., P. Friederichs, and M. Latif (2004), Tropical Pacific decadal variability and its relation to decadal modulations of ENSO, *J. Clim.*, *17*, 3761–3774.

Rodwell, M. J., and C. K. Folland (2002), Atlantic air-sea interaction and seasonal predictability, *Q. J. R. Meteorol. Soc.*, *128*, 1413–1443.

Rodwell, M. J., D. P. Rowell, and C. K. Folland (1999), Oceanic forcing of the wintertime North Atlantic Oscillation and European climate, *Nature*, *398*, 320–323.

Rotstayn, L. D., and U. Lohmann (2002), Tropical rainfall trends and the indirect aerosol effect, *J. Clim.*, *15*, 2103–2116.

Scaife, A. A., J. R. Knight, G. K. Vallis, and C. K. Folland (2005), A stratospheric influence on the winter NAO and North Atlantic surface climate, *Geophys. Res. Lett.*, *32*, L18715, doi:10.1029/2005GL023226.

Scaife, A. A., C. K. Folland, L. Alexander, A. Moberg, and J. R. Knight (2007), European climate extremes and the North Atlantic Oscillation, *J. Clim.*, in press.

Schlesinger, M. E., and N. Ramankutty (1994), An oscillation in the global climate system of period 65–70 years, *Nature*, *367*, 723–726.

Shabbar, A., J. Huang, and K. Higuchi (2001), The relationship between the wintertime North Atlantic Oscillation and blocking episodes in the North Atlantic, *Int. J. Climatol.*, *21*, 355–369.

Shindell, D. T., R. L. Miller, G. A. Schmidt, and L. Pandolfo (1999), Simulation of recent northern winter climate trends by greenhouse-gas forcing, *Nature*, *399*, 452–455.

Sigmond, M., P. C. Siegmund, E. Manzini, and H. Kelder (2004), A simulation of the separate climate effects of middle-atmospheric and tropospheric CO_2 doubling, *J. Clim.*, *17*, 2352–2367.

Smith, T. M., and R. W. Reynolds (2005), A global merged land and sea surface temperature reconstruction based on historical observations (1880–1997), *J. Clim.*, *18*, 2021–2036.

Stenchikov, G., K. Hamilton, R. J. Stouffer, A. Robock, V. Ramaswamy, B. Santer, and H.-F. Graf (2006), Arctic Oscillation response to volcanic eruptions in the IPCC AR4 climate models, *J. Geophys. Res.*, *111*, D07107, doi:10.1029/2005JD006286.

Stott, P. A., J. F. B. Mitchell, M. R. Allen, T. L. Delworth, J. M. Gregory, G. A. Meehl, and B. D. Santer (2006), Observational constraints on past attributable warming and predictions of future global warming, *J. Clim.*, *19*, 3055–3069.

Sud, Y. C., G. K. Walker, V. M. Mehta, and W. K.-M. Lau (2002), Relative importance of the annual cycles of sea surface temperature and solar irradiance for tropical circulation and precipitation: A climate model simulation study, *Earth Interact.*, *6*, 1–32.

Sutton, R. T., and D. L. R. Hodson (2005), Atlantic Ocean forcing of North American and European summer climate, *Science*, *309*, 115–118.

Sutton, R. T., B. Dong, and J. M. Gregory (2007), Land/sea warming ratio in response to climate change: IPCC AR4 model results and comparison with observations, *Geophys. Res. Lett.*, *34*, L02701, doi:10.1029/2006GL028164.

Thompson, D. W. J., and J. M. Wallace (2000), Annular modes in the extratropical circulation. Part 1: Month-to-month variability, *J. Clim.*, *13*, 1000–1016.

Thompson, D. W. J., and J. M. Wallace (2001), Regional climate impacts of the Northern Hemisphere annular mode, *Science*, *293*, 85–89.

Trenberth, K. E., and D. J. Shea (2006), Atlantic hurricanes and natural variability in 2005, *Geophys. Res. Lett.*, *33*, L12704, doi:10.1029/2006GL026894.

Vellinga, M., and P. Wu (2004), Low-latitude fresh water influence on centennial variability of the thermohaline circulation, *J. Clim.*, *17*, 4498–4511.

White, W. B., Y. M. Tourre, M. Barlow, and M. Dettinger (2003), A delayed action oscillator shared by biennial, interannual, and decadal signals in the Pacific Basin, *J. Geophys. Res.*, *108*(C3), 3070, doi:10.1029/2002JC001490.

Zhang, R., and T. L. Delworth (2006), Impact of Atlantic multidecadal oscillations on India/Sahel rainfall and Atlantic hurricanes, *Geophys. Res. Lett.*, *33*, L17712, doi:10.1029/2006GL026267.

Zhang, R., T. L. Delworth, and I. M. Held (2007), Can the Atlantic Ocean drive the observed multidecadal variability in Northern Hemisphere mean temperature?, *Geophys. Res. Lett.*, *34*, L02709, doi:10.1029/2006GL028683.

Zhang, Y., J. M. Wallace, and D. S. Battisti (1997), ENSO-like decadal variability over the Pacific sector, *J. Clim.*, *10*, 1004–1020.

P. Baines, Department of Civil and Environmental Engineering, University of Melbourne, Melbourne, Vic 3010, Australia.

A. Colman, C. Folland, J. Knight, D. Parker, and A. Scaife, Hadley Centre, Met Office, Exeter EX1 3PB, UK. (david.parker@metoffice.gov.uk)

B. Dong, Walker Institute for Climate System Research, University of Reading, Reading RG6 6BB, UK.